We are IntechOpen, the world's leading publisher of Open Access books
Built by scientists, for scientists

4,800
Open access books available

122,000
International authors and editors

135M
Downloads

154
Countries delivered to

Our authors are among the

TOP 1%
most cited scientists

12.2%
Contributors from top 500 universities

CLARIVATE ANALYTICS
BOOK CITATION INDEX
INDEXED

WEB OF SCIENCE™

Selection of our books indexed in the Book Citation Index
in Web of Science™ Core Collection (BKCI)

Interested in publishing with us?
Contact book.department@intechopen.com

Simultaneous Detection of Multi-DNAs and Antigens Based on Self-Assembly of Quantum Dots and Carbon Nanotubes

Peng Huang and Daxiang Cui
National Key Laboratory of Nano/Micro Fabrication Technology,
Key laboratory for thin film and microfabrication of Ministry of Education, Institute of
Micro and Nano Science and Technology, Shanghai Jiao Tong University, Shanghai,
P. R. China

1. Introduction

The development of convenient methodologies for simultaneous detection of specific multi-DNAs and antigens in biological and environmental samples has received broad attention because their detection, identification and quantification are very complex, expensive and time consuming (Abu-Salah et al., 2010; Strehlitz et al., 2008; Zhang et al., 2009). Over the past 30 years, biosensors, namely the devices incorporating biological sensing elements either intimately connected to or integrated within transducers, have been designed and fabricated to find effective solutions to these problems, which offer certain operational advantages over other traditional methods, notably with respect to rapidity, ease-of-use, low cost, simplicity, portability, and ease of mass manufacture (Cooper, 2002; Turner, 2000; Turner et al., 1987). The fundamental prerequisite of biosensors depends on specific molecular recognition based on affinity between complementary structures such as enzyme-substrate, antibody-antigen, receptor-hormone, and so forth (Zhang et al., 2009). This specific recognition gives rise to the production of concentration–proportional signals. Up to date, some biosensors have been commercialized for some special applications like blood glucose and lactate measurement or bioprocess control, amongst others. However, they have not still entered the market as much as expected, which is caused by the following reasons: (1) the selectivity and specificity of biosensor highly depends on biological recognition systems (Spichiger-Keller, 1998); (2) the sensitivity detection limit is difficult to achieve trace levels, even the single molecular detection (Sheehan and Whitman, 2005); (3) High throughput assay is desired to simultaneously process multiple samples (Sittampalam et al., 1997); (4) the biological recognition elements of the biosensor (e.g. enzymes, antibodies or cells) are usually instable (So et al., 2005).

With the development of nanoscience and nanotechnology, a series of novel nanomaterials with controlled size and morphologies are being fabricated, their novel properties are being gradually discovered with difference from their corresponding bulk materials, and the applications of nanomaterials in biosensors have also made great advances (Jianrong et al., 2004; Kumar, 2007; Pandey et al., 2008). Nanomaterials can be made from both inorganic and organic materials and are less than 100 nm in length along

at least one dimension (Asefa et al., 2009; Zhong, 2009). This small size scale leads to large surface areas and unique size-related optical properties. For example, the quantum confinement effects that occur in nanometer-sized semiconductors widen their band gap and generate well-defined energy levels at the band edges, causing a blue-shift in the threshold absorption wavelength with decreasing particle size and inducing luminescence that is strictly correlated to particle size (Krishna and Friesner, 1991; Peng et al., 2000). Therefore, the position of the absorption as well as the luminescence peaks can be fine-tuned by controlling the particle size and the size distribution during synthesis, generating a large group of "fluorophores" with diverse optical properties (Nirmal and Brus, 1999; Pradhan et al., 2005). The size- or shape-controllable optical characteristics of nanomaterials facilitate the selection of diverse probes for higher throughput assay (Zhong, 2009). Furthermore, the nanostructure can provide a substrate support for sensing assays with multiple probe molecules attached to each nanostructure, simplifying assay design and increasing the labeling ratio for higher sensitivity (Kumar, 2007). Therefore, nanomaterials have opened up new horizons for biosensors.

Biosensors based on nanomaterials, which represent the integration of material science, molecular engineering, chemistry and biotechnology, can markedly improve the sensitivity, selectivity, specificity and rapidity of bio-molecular detection, offer the promising capability of detecting or manipulating atoms and molecules, and have great potential in the development of the miniaturizebility or portability of analytical system (Zhang et al., 2009). Previous studies have shown that combining the specific molecular recognition ability of biomolecules with the unique structural and photophysical characteristics of inorganic or organic nanomaterials, such as nanocrystals, nanotubes, nanowires, nanomicelles, and nanovesicles, can create new types of analytical tools (Niemeyer, 2001). So far, the nanomaterials are widely used in biosensors mainly including (1) carbon nanomaterials (e.g., fullerenes, carbon nanotubes, carbon nanohorns, graphene, etc.) (Chen et al., 2003; Vamvakaki and Chaniotakis, 2007; Yang et al., 2010b), (2) metallic nanomaterials (e.g., quantum dots, gold nanoparticles, gold nanorods, europium nanoparticles, etc.) (Ao et al., 2006; Liu, 2009; Pan et al., 2005), (3) silica nanomaterials (Slowing et al., 2007), (4) organic polymer nanomaterials (e.g., molecular imprinted polymers) (Hatchett and Josowicz, 2008), or (5) supramolecular aggregates (nanomicelles, nanovesicles) (Kuhn, 1994). Fig. 1 illustrates the correlation between these typical nanomaterials and the major properties exploited for analytical purposes (Valcarcel et al., 2008).

2. Carbon nanotubes as analytical tools

Since their discovery by Iijima in 1991, Carbon nanotubes (CNTs), due to the remarkable structure-dependent electronic, mechanical, optical, and magnetic properties, have triggered intensive studies directed towards numerous applications including nanoelectronics, biomedical engineering, biosensing, and bioanalysis (Dai, 2002; Iijima, 1991). CNTs are rolled up seamless cylinders of graphene sheets. According to the number of graphene layers, CNTs are classified into single-walled carbon nanotubes (SWNTs) and multi-walled carbon nanotubes (MWNTs) (Liu et al., 2009). Their lengths can range from several hundred nanometers to several micrometers, and the diameters from 0.2 to 2 nm for SWNTs and from 2 to 100 nm for coaxial MWNTs (Valcarcel et al., 2005). So far, CNTs has been used as an analytical tool to improving the analytical process (Valcarcel et al., 2007). CNTs-based biosensors have been developed to detect biological species including proteins and DNA.

Fig. 2 illustrates their potential roles in the development of new tools for analytical science, arranged in terms of complexity of design and integration (Valcarcel et al., 2007).
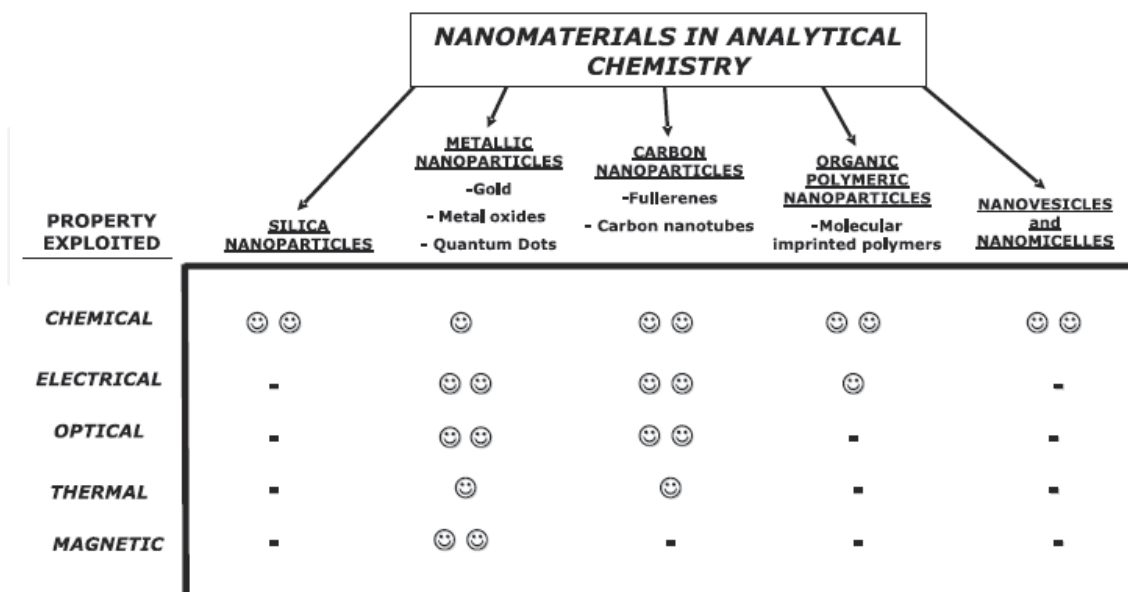
PROPERTY EXPLOITED	NANOMATERIALS IN ANALYTICAL CHEMISTRY				
	SILICA NANOPARTICLES	METALLIC NANOPARTICLES -Gold - Metal oxides - Quantum Dots	CARBON NANOPARTICLES -Fullerenes - Carbon nanotubes	ORGANIC POLYMERIC NANOPARTICLES -Molecular imprinted polymers	NANOVESICLES and NANOMICELLES
CHEMICAL	☺ ☺	☺	☺ ☺	☺ ☺	☺ ☺
ELECTRICAL	-	☺ ☺	☺ ☺	☺	-
OPTICAL	-	☺ ☺	☺ ☺	-	-
THERMAL	-	☺	☺	-	-
MAGNETIC	-	☺ ☺	-	-	-

Fig. 1. Correlation between typical nanomaterials and the major property exploited for analytical purposes (Valcarcel et al., 2008). (With permission from Springer)
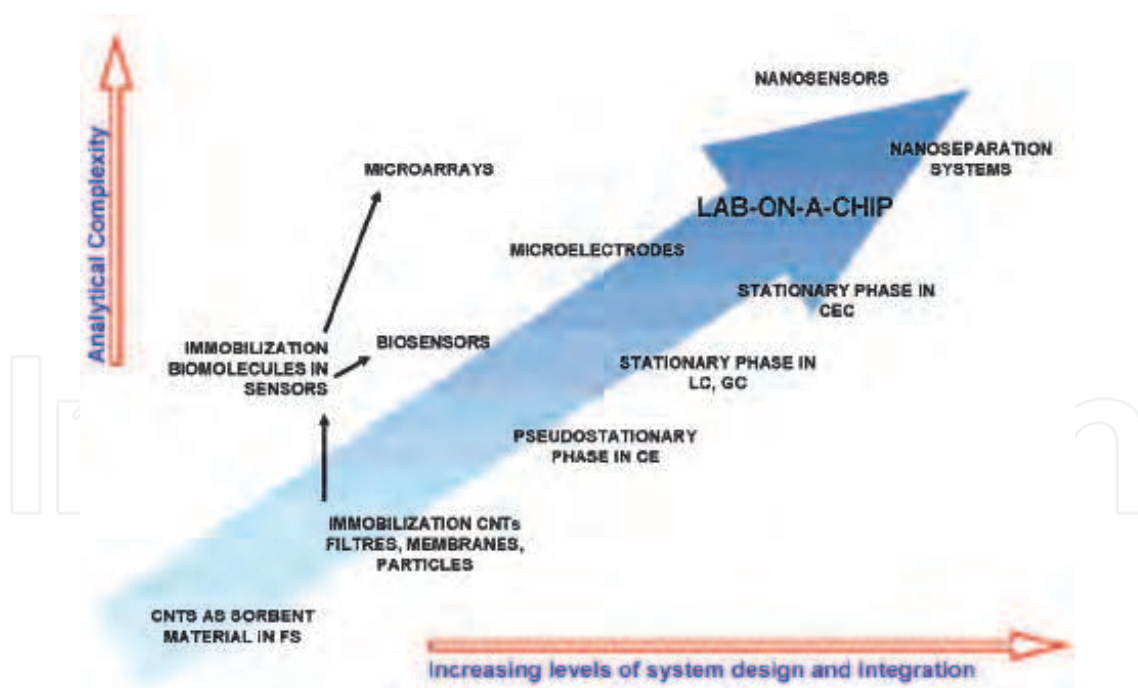

Fig. 2. Classification of analytical tools based on the use of carbon nanotubes according to the analytical complexity and the increasing level of system design and integration (Valcarcel et al., 2007). (With permission from American Chemical Society)

Generally, CNTs are expected to be controllably assembled into designed architectures as integral components of composites or supramolecular structures (Grzelczak et al., 2006). The

integration of biomaterials (e.g., proteins/enzymes, antigens/antibodies, or DNA) with CNTs provides new hybrid systems that combine the conductive or semiconductive properties of CNTs with the recognition or catalytic properties of the biomaterials in Fig. 3 (Katz and Willner, 2004). CNTs can provide scaffolds for biomolecules immobilization, allowing subsequent applications in biosensors, utilizing the intrinsic electronic or optical properties of CNTs for signal transduction (Cataldo, 2008). Due to CNTs' the high surface area, semiconducting behavior, band gap fluorescence, and strong Raman scattering spectra, the proximal or adsorbed biomolecules can be measured or detected easily, when their interactions along the CNTs sidewall, at functionalized cap regions (Cheung et al., 1998), and even within the nanotube shell (Lin et al., 2004; Liu et al., 2009). Proximity of reasonably charged or polarized biomolecules yields gating effects on isolated semiconducting CNTs, or net semiconducting networks of CNTs, thus yielding field-effect transistors (FETs) capable of quantifying the degree of specific or non-specific binding of biomolecules (Chen et al., 2003; Liu et al., 2009). Additionally, CNTs were also used as analytical targets. After specific conjugation of targeting ligands to SWNT tags or coupled with sufficient sidewall passivation in order to prevent non-specific binding, the photoluminescent (FL) and Raman scattering properties of SWNTs can be detected as target signals in biosensors (Liu et al., 2009; Valcarcel et al., 2007). Therefore, CNTs are of great interest for the development of highly sensitive and multiplexed biosensors for applications in analytical chemistry.
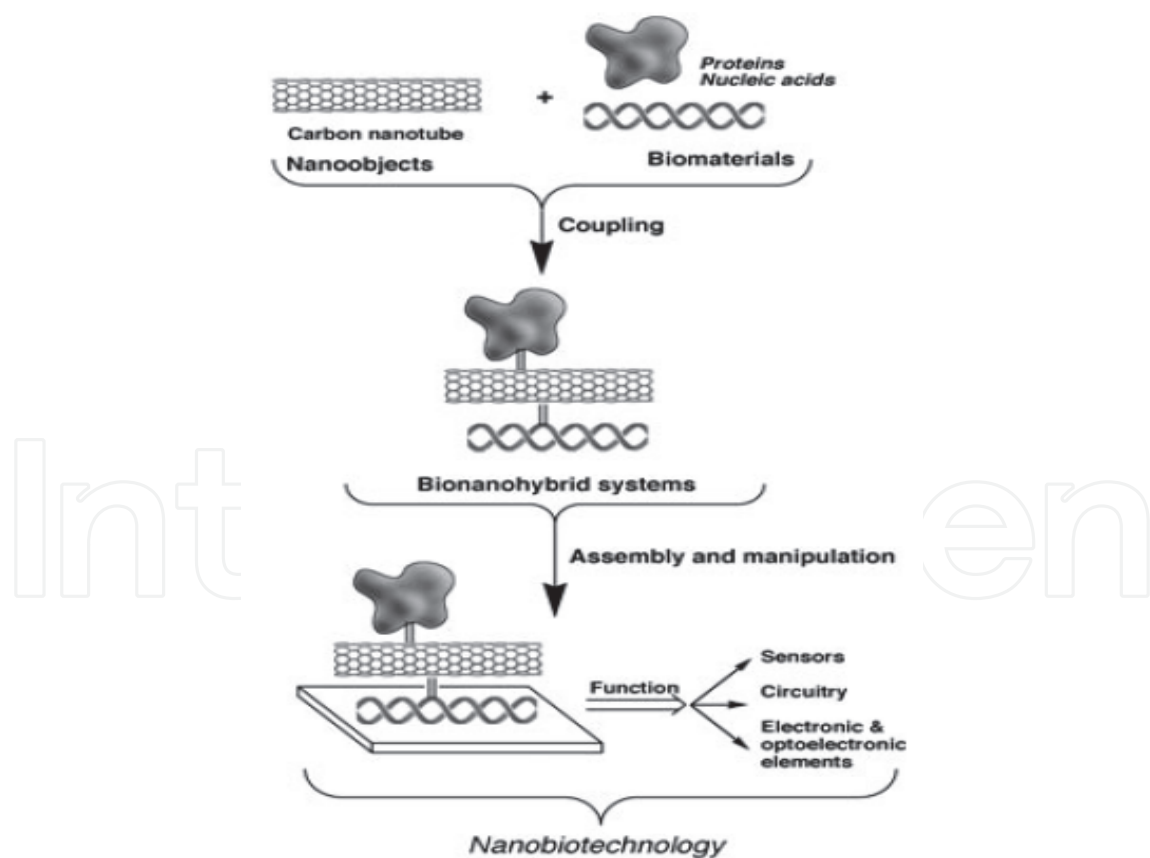

Fig. 3. The conceptual generation of biomolecules-carbon nanotubes conjugates, and their assembly to yield functional devices (Katz and Willner, 2004). (With permission from Wiley-VCH)

Simultaneous Detection of multi-DNAs and Antigens
Based on Self-Assembly of Quantum Dots and Carbon Nanotubes
245

3. Quantum dots as analytical tools

Since their discovery in the early 1980s, semiconductor nanomaterials or quantum dots (QDs), have been extensively used as potential luminescence probes due to their high resistance to photobleaching, narrow emission spectra, broad excitation spectra, and longer fluorescence lifetime in the field of biosensing and imaging (Alivisatos, 1996). QDs are usually composed of atoms of elements from groups II to VI (e.g., Cd, Zn, Se, Te) or III–V (e.g., In, P, As) in the periodic table (Chan et al., 2002). As a result of their very small (< 10 nm) dimensions, QDs exhibit quantum confinement effects that are responsible for their wide UV-visible absorption spectra, narrow emission bands, and optical properties, which can be tuned by size, composition, and shape (Alivisatos, 2003; Chan and Nie, 1998). These features come with high flexibility in the selection of excitation wavelength as well as minimal overlap in the emission spectra from multiple QDs, making them excellent labels for high throughput screening (Chan et al., 2002; Han et al., 2001). Additionally, choosing excitation wavelengths far from the emission wavelengths can eliminate background scattering.

Compared with organic fluorophores, QDs have similar quantum yields but extinction coefficients that are 10~50 times larger, and much-reduced photobleaching rates. The overall effect is that QDs have 10~20 times brighter fluorescence and about 100~200 times better photostability (Gao et al., 2005; Zhong, 2009). For applications in biomedical studies, QDs should be water soluble, which can be achieved in two ways: the first is to directly synthesize QDs in aqueous solution; the other is to synthesize QDs in organic solvents and then transfer the hydrophobic QDs into aqueous solution, for example, by ligand exchange or polymer coating (Zhang et al., 2010). So far, several methods have been developed to synthesize water-soluble quantum dots for use in cellular imaging, immunoassays, DNA hybridization and optical bar-coding (Drbohlavova et al., 2009; Yang et al., 2009). Moreover, QDs also have been used to study the interaction between protein molecules or detect the dynamic course of signal transduction in live cells by fluorescence resonance energy transfer (FRET) (Chan and Nie, 1998).

Because QDs are intrinsically fluorescent, they can be widely employed as the reporter molecules for biomolecules detection (Chan and Nie, 1998). For example, QDs-based western blot detection kits can improve the sensitivity detection limit as low as 20 pg protein per lane (Ornberg et al., 2005). The detection limits is around hundreds of picograms of protein per lane in the colorimetric or chemiluminescent detection. So the QDs-based protocol is more sensitive with better image quality in the same measuring time. The test samples can be stored for longer time after staining with minimal loss of signal (Edgar et al., 2006). According to the high resistance of QDs to photobleaching, Genin et al. have reported that the organic dye CrAsH conjugated QDs nanohybrids serve as a probe to bind efficiently and selectively to Cys-tagged proteins and subsequently trace them for more than 150 s, where the fluorescence emission of CrAsH displayed a significant increase after the interaction between CrAsH and cysteine (Genin et al., 2008). While the latter faded rapidly under continuous excitation, emission of the QDs remained unaffected. The persistent fluorescence of the QDs should thus allow extended monitoring of the target protein. In particular, the use of multicolor QDs probes in immunohistochemistry (IHC) is considered one of the most important and clinically relevant applications. Nie et al. have developed antibody-conjugated QDs for multiplexed and quantitative (or semi-quantitative) IHC, and have achieved five-color molecular profiling on formalin-fixed and paraffin-embedded

(FFPE) clinical tissue specimens (Xing et al., 2007). They have also optimized the experimental procedures for QDs bioconjugation (**Fig. 4**), tissue specimen preparation, multi-color staining, image processing and analysis, and biomarker quantification.
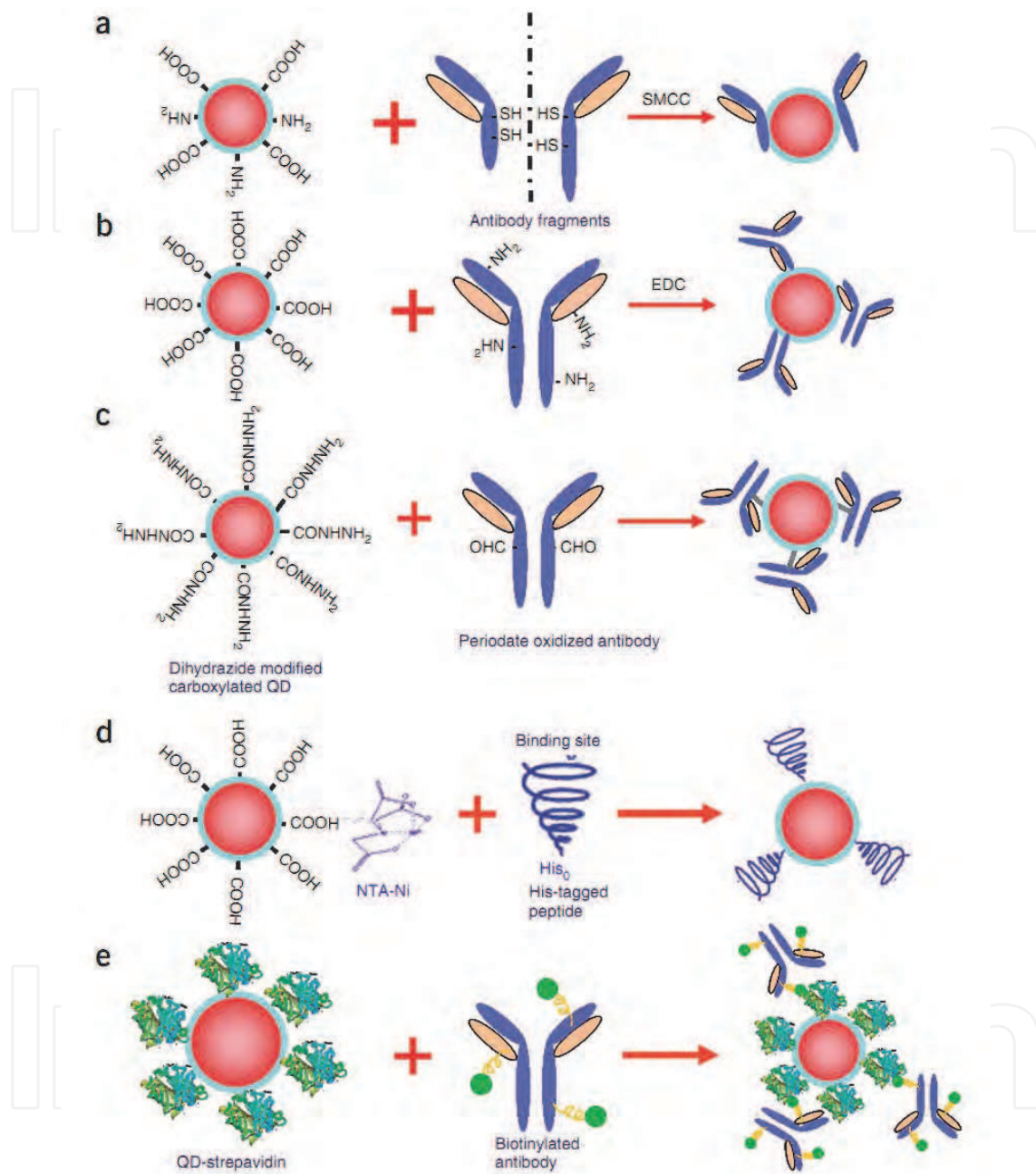

Fig. 4. Schematic diagrams showing various methods for QDs-antibody (QD-Ab) bioconjugation. (a)QDs conjugation to antibody fragments via disulphide reduction and sulfhydryl-amine coupling; (b) covalent coupling between carboxylic acid (-COOH) coated QDs and primary amines (-NH$_2$) on intact antibodies using EDAC as a catalyst; (c) site-directed conjugation via oxidized carbohydrate groups on the antibody Fc portion and covalent reactions with hydrazide-modified QDs; (d) conjugation of histidine-tagged peptides or antibodies to Ni-NTA modified QDs; and (e) noncovalent conjugation of streptavidin-coated QDs to biotinylated antibodies (Xing et al., 2007). (With permission from Nature)

Recently, our group have reported a quick and parallel analytical method based on QDs for ToRCH-related antibodies including Toxoplasma gondii, Rubella virus, Cytomegalovirus and Herpes simplex virus type 1 (HSV1) and 2 (HSV2) (Yang et al., 2009). We fabricated the microarrays with the five kinds of ToRCH-related antigens and used CdTe QDs to label secondary antibody and then analyzed 100 specimens of randomly selected clinical sera from obstetric outpatients (**Fig. 5**). In comparison with enzyme-linked immunosorbent assay (ELISA) kits, the QDs labeling-based ToRCH microarrays display comparable sensitivity and specificity with ELISA. Besides, the microarrays hold distinct advantages over ELISA test format in detection time, cost, operation and signal stability.
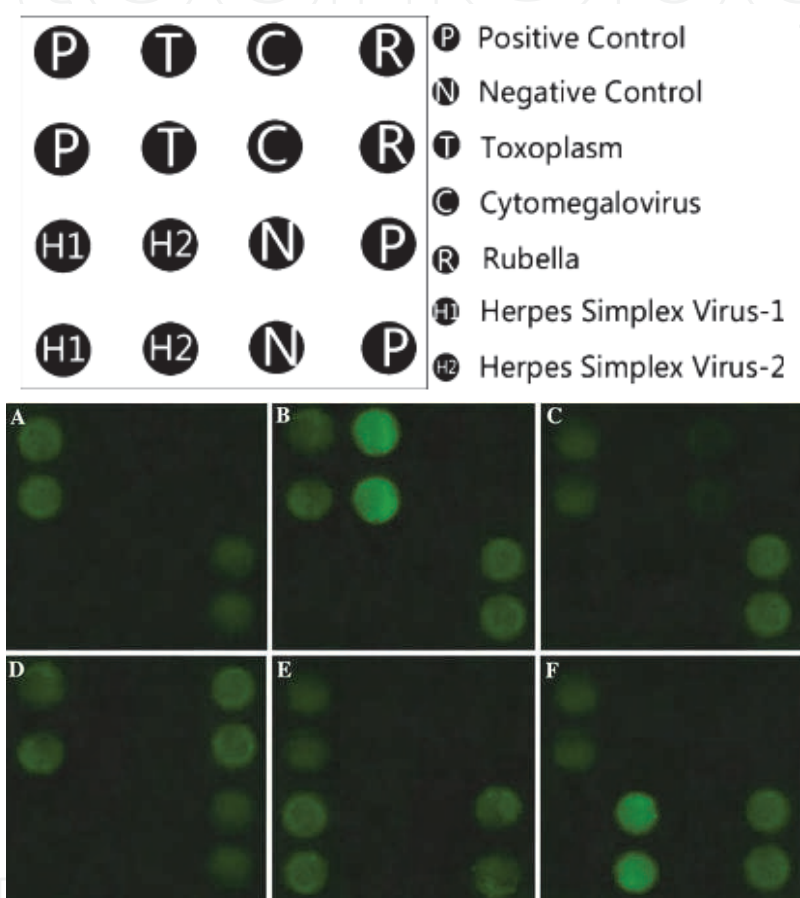

Fig. 5. The microarray results with corresponding control sera (a negative serum; b positive control serum of Toxoplasmosis; c positive control serum of Cytomegalovirus; d positive control serum of Rubella virus; e positive control serum of Herpes simplex virus type 1; f positive control serum of Herpes simplex virus type 2) (Yang et al., 2009). (With permission from Springer)

Additionally, we developed a novel fluorescent POC (Point Of Care) test method to be used for screening for syphilis, combining the rapidness of lateral flow test and sensitiveness of fluorescent method (Yang et al., 2010a). 50 syphilis-positive specimens and 50 healthy specimens conformed by Trep-onema pallidum particle agglutination (TPPA) were tested with QDs-labeled and colloidal gold-labeled lateral flow test strips, respectively. Our results showed that both sensitivity and specificity of the QDs–based method reached up to 100% (95% confidence interval [CI], 91~100%), while those of the colloidal gold-based method

were 82% (95% CI, 68–91%) and 100% (95% CI, 91–100%), respectively. We found that the naked-eye detection limit of QDs–based method could achieve 2 ng/mL of anti-TP47 polyclonal antibodies purified by affinity chromatography with TP47 antigen, which was ten-fold higher than that of colloidal gold–based method (**Fig. 6**).
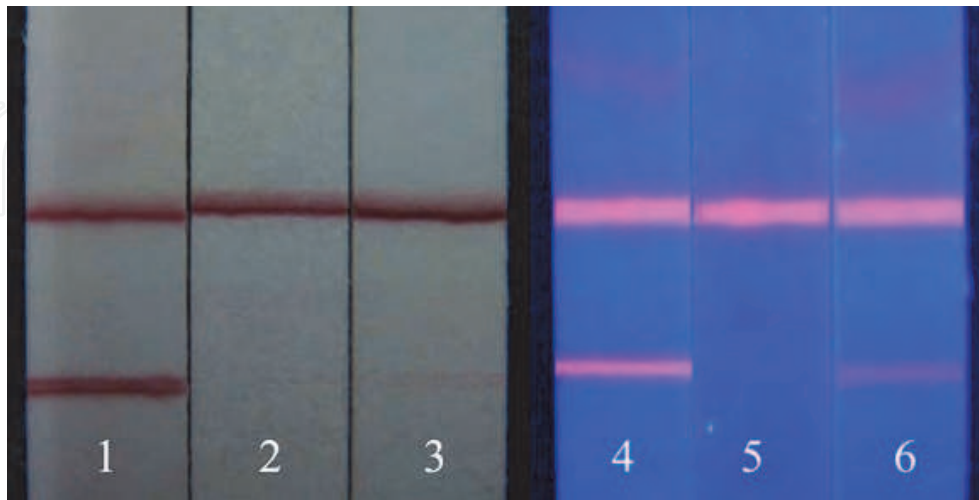

Fig**. 6.** Result of detection of clinical specimens by colloidal gold and QDs (Yang et al., 2010a). result of detection by colloidal gold: 1 positive; 2 negative; 3 weak positive; result of detection by QDs: 4 positive; 5 negative; 6 weak positive. (With permission from Springer)

Due to their bright intensity and high photostability, QDs also have a wide range of applications in bioimaging (Cui et al., 2009). Our group has successfully prepared the dendrimer-modified QDs with water-soluble, high quantum yield, and good biocompatibility. Our results indicated that arginine-glycine-aspartic acid (RGD) conjugated QDs can specifically target human umbilical vein endothelial cells (HUVEC) and A375 melanoma cells, as well as nude mice loaded with A735 melanoma cells (Li et al., 2010b). Meanwhile, we have successfully synthesized dendrimer-modified QDs nanocomposites, and developed a class of aptamers-conjugated nanoprobes, which could specifically bind with U251 glioblastoma cells and exhibit in vitro molecular imaging (Li et al., 2010a).

4. Carbon nanotubes and quantum dots nanohybrids as analytical tools

Sensitive detection of target analytes present at trace levels in biological samples often requires the labeling of reporter molecules with fluorescent dyes, because fluorescence detection is by far the dominant detection method in the field of sensing technology, due to its simplicity, the convenience of transducing the optical signal, the availability of organic dyes with diverse spectral properties, and the rapid advances made in optical imaging (Zhong, 2009). However, it can be difficult to obtain a low detection limit in fluorescence detection due to the limited extinction coefficients or quantum yields of organic dyes and the low dye-toreporter molecule labeling ratio.

Currently, fluorescence (Förster) resonance energy transfer (FRET) and photoinduced electron transfer (PET) have been widely studied as novel fluorescence detection techniques in biosensors (Zhang et al., 2010). In FRET sensing systems, QDs normally act as donor and transfer excitation energy to a vicinal fluorophore acceptor, leading to a reduced donor PL and a concomitant increased acceptor PL (**Fig. 7**). In PET sensing systems, the excited QDs

Simultaneous Detection of multi-DNAs and Antigens
Based on Self-Assembly of Quantum Dots and Carbon Nanotubes
249

act as the electron donor and transfer the excited electrons to acceptor molecules. This in turn results in a quenched QD PL and an increased acceptor PL (if possible). In both, FRET and PET sensing systems, the most significant advantage is that the transfer efficiencies can be used as a ratiometric readout without demanding an extra reference. The second advantage is that such sensing systems are more flexible and enable more complicated designs, resulting from the multiple components involved, e.g., donor, acceptor, and spacers.
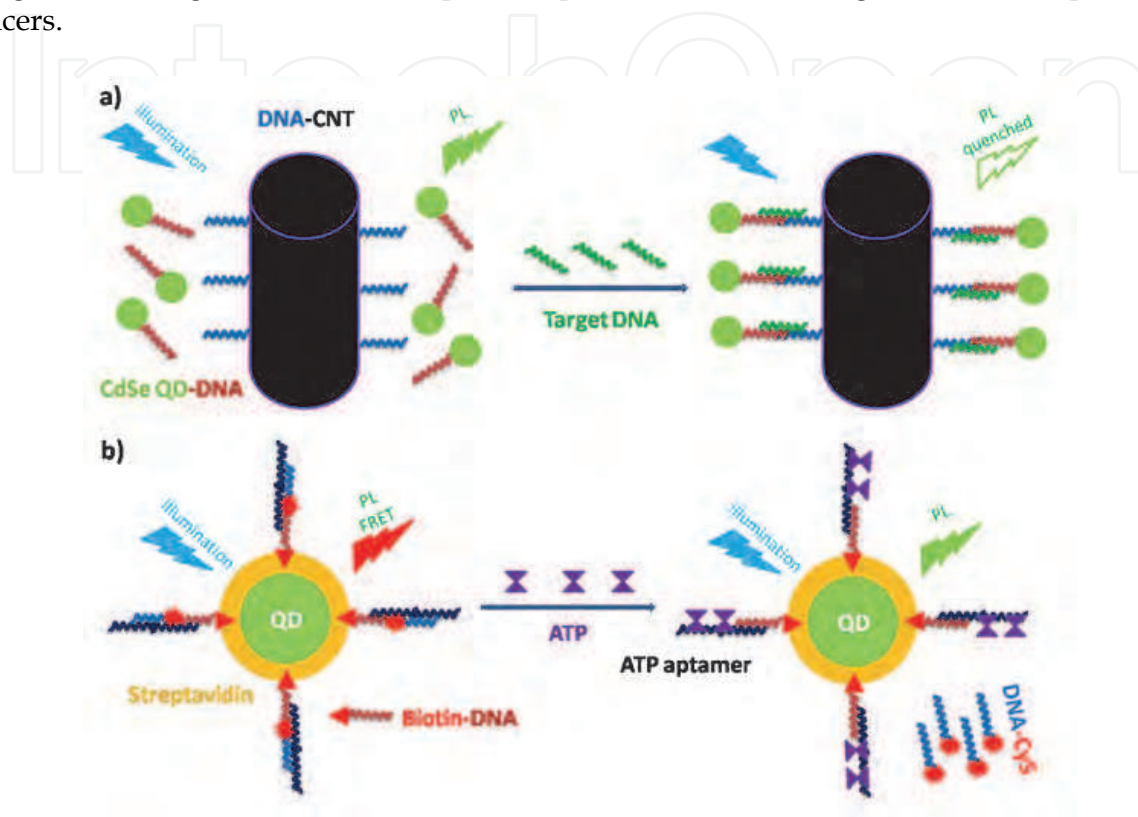
Fig. 7. FRET-based sensing (Zhang et al., 2010). a) CdSe QDs and CNTs are conjugated with two oligonucleotides. The two oligonucleotides can be hybridized upon binding a target DNA fragment. In the absence of target DNA, the QDs have its original PL. In the presence of the target DNA fragment, hybridization brings QDs and CNTs close enough so that the QDs PL is quenched by the CNTs. b) Streptavidin modified commercial QDs 'decorated' with biotinylated DNA fragments. An ATP aptamer binds with one side to the DNA attached to the QDs and with one side to Cy5-labeled DNA. Upon excitation of the QDs donor, FRET reduces the QDs PL and increases the PL of the Cy5 acceptor. In the presence of ATP molecules, the aptamer dehybridizes and complexes the ATP. As soon as the Cy5-labeled DNA becomes detached from the ATP aptamer, the distance to the QDs is increased and there is no longer FRET. (With permission from Springer)

Based on FRET, Wang et al. combined positively charged CdTe QDs capped with cyst-amine with negatively charged gold nanoparticles (GNPs) capped with 11-mercaptoundecanoic acid (MUA) in a FRET system, the PL of donor QDs can be quenched by the close acceptor GNPs, which is due to the high extinction coefficient and broad absorption of GNPs (Wang and Guo, 2009). Firstly, QDs and GNPs assemble into aggregates due to their mutual electrostatic attraction. Then the Pb^{2+} was added, MUA-modified GNPs chelated with it into aggregates, the QDs were released and the restored PL was read out. Finally, the PL changes of the QDs

were instead of detecting changes. QD-based FRET sensors have been investigated by Mattoussi (Medintz et al., 2003) and Willner (Patolsky et al., 2003) groups. Our group also designed a unique, sensitive, and highly specific fluoroimmunoassay system for antigen detection using GNPs and QDs nanoparticles (Huang et al., 2010). To demonstrate its analytical capabilities, the CdTe QDs were coated with anti-HBsAg monoclonal antibodies (QDs-MAb1) and GNPs coated with another anti-HBsAg monoclonal antibodies (GNPs-MAb2) which specifically bound with HBsAg could sandwich the HBsAg captured by the immunoreactions. The sandwich-type immunocomplex was formed and the fluorescence intensity of QDs was measured. The results showed that the fluorescence intensity of QDs at 570 nm was negative linear proportional to the HBsAg concentration logarithm, and the limit of detection of the HBsAg was 0.928 ng/mL. This new system can be extended to detect target molecules with matched antibodies and has broad potential applications in immunoassay and disease diagnosis.

CNTs represent one type of unique nanomaterials used in fluorescence-based bioassays. The sensing utilizes the ability of CNTs to quench organic dyes or QDs (Pan et al., 2006b; Pan et al., 2008). Tang group reported that organic dyes could be quenched by CNTs through an energy transfer mechanism (Yang et al., 2008). This feature was employed to develop a non-covalent assembly between CNT and ssDNA for effective sensing of biomolecule interactions (Fig. 8). The strong interaction between CNT and ssDNA quenched the fluorophore conjugated on ssDNA. Hybridization of a complimentary DNA strand or binding of an interactive protein caused ssDNA to be released from the CNT, leading to the restoration of fluorescence signal in increments relative to the fluorescence without a target. The signaling mechanism makes it possible to detect the target by fluorescence spectroscopy.
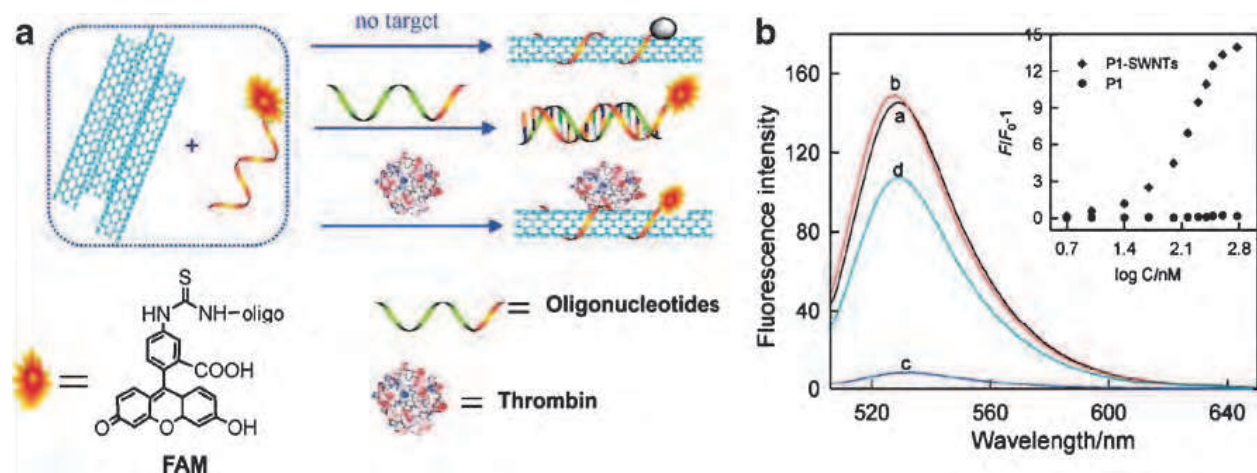

Fig. 8. A Scheme for signaling biomolecular interactions using an assembly between SWNTs and dye-labeled ssDNA. P1 and P2, the FAM-labeled oligonucleotides; P2, the thrombin-binding aptamer; T1 and T2, the perfect cDNA (T1) and one mismatched DNA (T2) of P1. B Fluorescence emission spectra (λ_{ex}=480 nm) of P1 (50 nM) under different conditions: (a) P1 in PBS; (b) P1 + 300 nM T1; (c) P1 + SWNTs; and (d) P1 + SWNTs + 300 nM T1. Inset: fluorescence intensity ratio of P1 (b) and P1-SWNTs with F/F_0−1 plotted against the logarithm of the concentration of T1 (Yang et al., 2008; Zhong, 2009). (With permission from American Chemical Society and Springer)

Recently, nanohybrids containing both semiconductor QDs and CNTs have been the subject of great interest as a consequence of the development of methods for the chemical

modification of CNTs and the seeking for novel functional materials in biosensors (Cui, 2007; Pan et al., 2009). When QDs were binding to CNTs, CNTs could promote direct charge transport and efficient charge transfer from the QDs. This system has the potential to significantly increase the efficiency of photovoltaic devices (Kamat, 2007). Besides, CNTs binding with QDs together can provide one kind of novel nanomaterials–luminescent CNTs can afford fluorescent labels and be utilized for real-time detection, molecular imaging and cell sorting in biological applications (Guo et al., 2008; Shi et al., 2006). Our group has synthesized luminescent CNTs as a new functional platform for bioanalytical sciences and biomedical engineering (Cui et al., 2010).

To further understand that how the nanohybrid structure affects the charge transfer and energy transfer behaviors between the QDs and CNTs, the interactions between QDs (such as CdS, CdSe and CdTe) and CNTs have been carefully investigated by several groups (Guldi et al., 2006; Li et al., 2006b; Robel et al., 2005; Sheeney-Haj-Ichia et al., 2005; Si et al., 2009). The charge-transfer efficiencies were evaluated by studying the changes in the photoluminescence (Li et al., 2006b) or photo-electrochemical properties of hybrid materials (Pan et al., 2008). Studies indicated that strong PL quenching by charge-transfer mechanism were found in the CdS/TOAB/CNT (Guldi et al., 2005), CdSe/pyridine/CNT (Li et al., 2006a) and CdSe/pyrene/CNT (Hu et al., 2008) system. Partial emission quenching was observed on nanohybrids consisting of dendron-modified CdS QDs on CNTs (Hwang et al., 2006). In contrast, Marek Grzelczak et al. reported a reproducible procedure based on the combination of both polymer wrapping and LbL self-assembly techniques for the deposition of CdTe nanocrystals onto CNTs, yielding linear colloidal CdTe–CNT composites with a high degree of coverage (Grzelczak et al., 2006). Although quenching of PL from CdTe occurs when the nanocrystals are directly assembled on the CNTs, such quenching can be controlled through the growth of a silica-shell spacer between the CNT surface and the deposited QDs. The main general steps of this method for the deposition of CdTe QDs onto CNTs and onto silica-coated CNTs (CNTs@SiO$_2$) are summarized in Fig. 9.
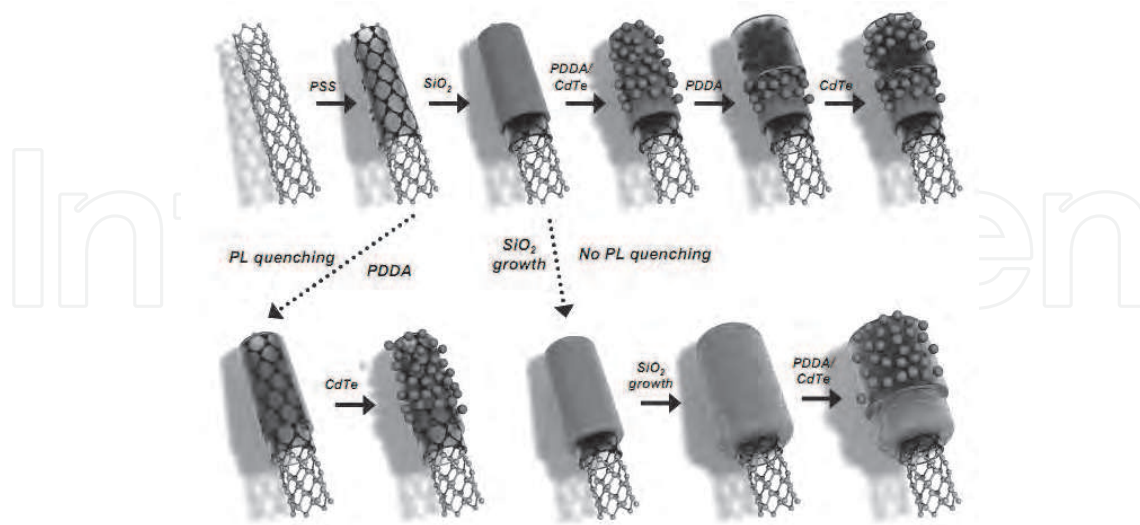

Fig. 9. Various possible routes for the preparation of CdTe-CNT and CdTe–CNT@SiO$_2$ nanocomposites. PSS: poly (sodium 4-styrene sulfonate); PDDA: poly (diallyldimethylammoniumchloride) (Grzelczak et al., 2006). (With permission from Wiley-VCH)

The previous works have shown that the PL properties of the QD/CNT nanohybrids are strongly dependent on QD-CNT separation, but precise control to the distance between QDs and CNT was difficult to achieve in the available systems. Recently, Hao-Li Zhang et al. reported a facile strategy for attaching CdSe QDs onto CNT surface by electrostatic self-assembly (Fig. 10) (Si et al., 2009). By using different mercaptocarboxylic ligands, the shell thicknesses of the CdSe QDs are well controlled within angstrom-level precision. The efficiency of the PL quenching decreases upon increasing the shell thickness due to the distance-dependent electron transfer efficiency. This work demonstrates that the shell thickness control to the QDs opens up a straightforward methodology for investigating the interaction between fluorescent nanomaterials coupled with CNTs.
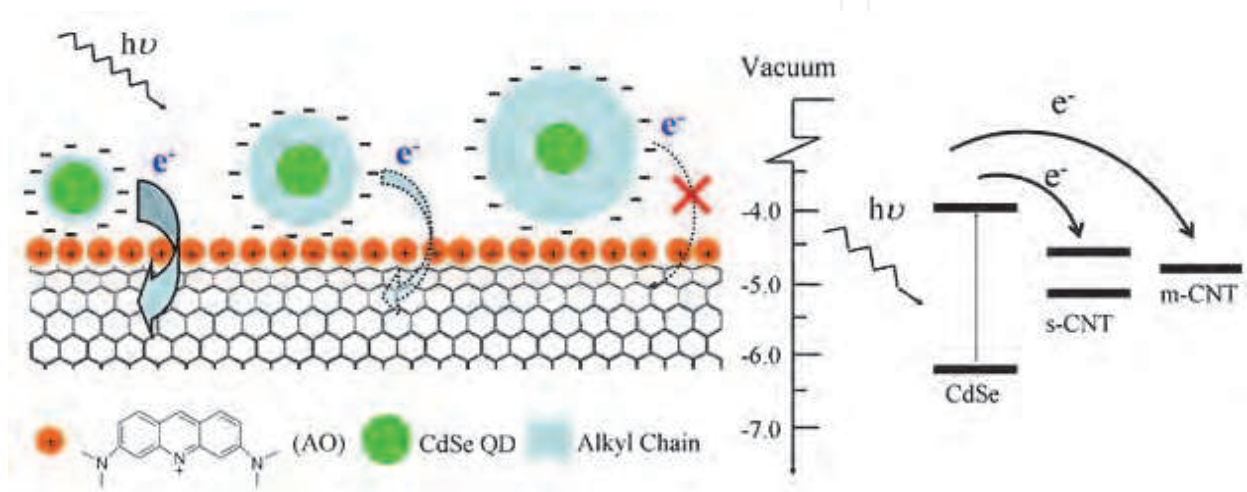

Fig. 10. Schematic illustration to the structures of the CdSe/CNT nanohybrids prepared by electrostatic assembly (left). The photo-induced charge-transfer efficiency within the nanohybrids is controlled by the shell thickness. Energy-level diagram and possible charge-transfer process for the conjugate complex between CdSe QDs and semiconducting CNTs (s-CNT) or metallic CNTs (m-CNT) are illustrated in the right (Si et al., 2009). (With permission from Springer)

An investigation of the effects of MWNTs on the PL properties of CdSe QDs showed that CNTs could suppress the PL of QDs through both dynamic and energy transfer quenching mechanisms (Cui et al., 2008; Pan et al., 2006b; Pan et al., 2008). In order to potentially exploit this feature in bioassays, we reported a novel ultrasensitive DNA or antigen detection strategy based on the CNT-QD assembly (Cui et al., 2008). MWNTs and QDs, their surfaces functionalized with oligonucleotide DNA or antibody (Ab), can be assembled into nanohybrid structure upon the addition of a target complementary oligonucleotide or antigen (Ag). Nanomaterials building blocks that vary in chemical composition, size, or shape are arranged in space on the basis of their interactions with complementary linking oligonucleotides for potential application in biosensors. We show how this oligonucleotide-directed assembly strategy could be used to prepare binary (two-component) assembly materials comprising two differently shaped oligonucleotide-functionalized nanomaterials. Importantly, the proof-of-concept demonstrations reported herein suggest that this strategy could be extended easily to a wide variety of multicomponent systems.

Simultaneous Detection of multi-DNAs and Antigens
Based on Self-Assembly of Quantum Dots and Carbon Nanotubes
253

5. Experimental section

5.1 Preparation of water-soluble CdSe QDs

The colloidal CdSe QDs were dissolved in chloroform and reacted with glacial mercaptoacetic acid (1.0 M) for 2 h. Water was added to this reaction mixture at a 1:1 volume ratio. After vigorous shaking and mixing, the chloroform and water layers separated spontaneously. The aqueous layer, which contained mercaptoacetic-coated QDs, was extracted (Scheme 1). Excess mercaptoacetic acid was removed by four or more rounds of centrifugation.
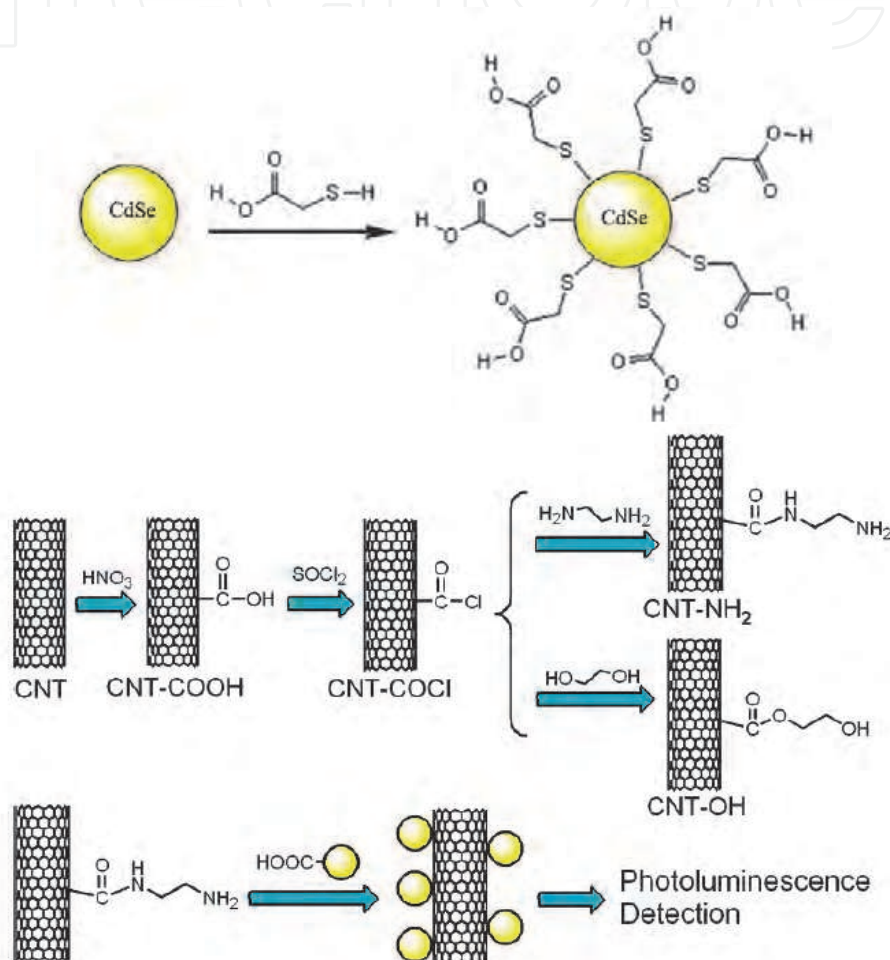
Scheme 1. Water-Soluble CdSe QDs, Preparation of CNT-COOH, CNT-OH, and CNT-NH₂, and Electrostatic Interaction between CNT-NH₂ and QDs. (With permission from American Chemical Society)

5.2 Preparation of CNT-COOH, CNT-OH, and CNT-NH₂

A 100 mg amount of pristine CNTs was added to aqueous HNO_3 (10.0 mL, 60%). The mixture was placed in an ultrasonic bath for 30 min and then stirred for 24 h while being boiled under reflux. The mixture was then in vacuum filtered through a 0.22 μm Millipore polycarbonate membrane and subsequently washed with distilled water until the pH of the filtrate was ca. 7. The filtered solid was dried under vacuum for 12 h at 60 °C. Dried CNT-COOH was suspended in $SOCl_2$ (20 mL) and stirred for 24 h at 65 °C. The solution was

filtered, washed with anhydrous THF, and dried under vacuum at room temperature for 24 h, generating CNT-COCl. Dried CNT-COCl was mixed with excess ethylene glycol and stirred for 48 h at 120 °C. The resulting solid was separated by vacuum filtration using a 0.22 µm Millipore polycarbonate membrane filter and subsequently washed with anhydrous THF. After repeated washing and filtration, the resulting solid was dried overnight in a vacuum, generating CNT-OH. On the other hand, CNT-COCl was reacted with ethylenediamine to obtain CNT-NH$_2$ (Scheme 1).

5.3 Preparation of CNT-DNA probe (Scheme 2)

Binding of the aminoalkyloligonucleotide, in PBS buffer (0.1 M NaCl, 10 mM phosphate buffer, pH 7.0), to the CNT was accomplished by adding 50 µL of 1 µM aminoalkyloligonucleotide to 1.0 mL of 1 mg/L CNT-COCl in phosphate buffer solution (PBS), incubated for 40 h at 25 °C, collected by centrifugation at 4000 rpm for 10 min, and resuspended in 1 mL PBS to form CNT-oligonucleotide composite (probe 1).
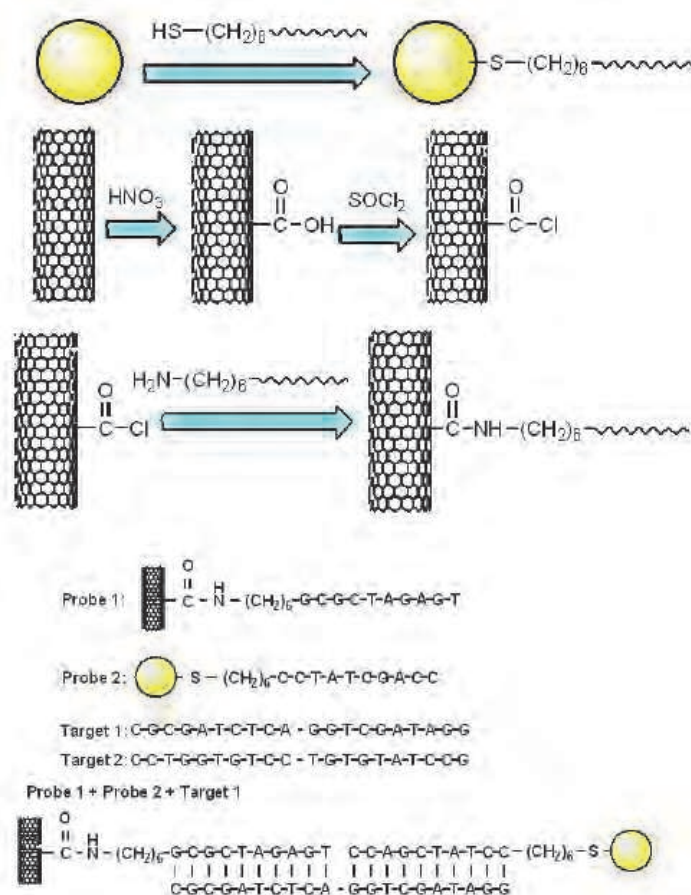
Scheme 2. Surface functionalization with oligonucleotide, and subsequent addition of target oligonucleotide to form CNT-QD assembly. Target 1, complementary DNA; target 2, non-complementary DNA. (With permission from American Chemical Society)

5.4 Preparation of QD-DNA probe

The colloidal CdSe QDs were dissolved in chloroform and were reacted with glacial mercaptoalkyloligonucleotide (1.0 µM) for 2 h. PBS buffer was added to this reaction mixture

at a 1:1 volume ratio. After vigorous shaking and mixing, the chloroform and PBS buffer layers separated spontaneously. The PBS buffer layer, containing mercaptoalkyloligonucleotide-coated QDs (probe 2), was extracted from chloroform liquid.

5.5 Preparation of CNT-Ab probe
For the covalent immobilization of antibody on the CNT surface, CNT-NH$_2$ was exposed to 20 nM anti-BRCAA1 IgG in PBS buffer (pH 7.4) overnight at room temperature, rinsed thoroughly in deionized water for 6 h, and then dried with nitrogen gas.

5.6 Preparation of QD-Ab probe
The QDs-pAb probes were prepared by adding BRCAA1 pAb (40 μg) to an aqueous solution of QDs (5 mL, 2.33 nM) at pH 9.0 for 30 min. Then, the solution was treated with 0.5 mL 10% BSA solution for a night to passivate and stabilize the QDs. The final QDs-pAb probes were re-dispersed in 0.01 M PBS at pH 7.4. CNTs-pAb probes also were prepared by above-mentioned method, and the pAb concentration was 1.5 mg/mL.

5.7 Photoluminescence (PL) measurement of CdSe QDs binding to CNTs
CNTs with concentrations from 0 to 100 mg/L were added to the CdSe aqueous solution. QD-CNT solutions were incubated at room temperature in the dark for 3 h. PL spectra were taken with a Perkin-Elmer LS-55 spectrofluorometer. Samples were thermostated at 25 °C. An excitation wavelength of 460 nm was used. The emission spectra were recorded from 500 to 650 nm. The excitation and emission slit widths were set to 5 and 5 nm, respectively. Samples were contained in 1 cm path length quartz cuvettes and continuously stirred. For control experiments, CNTs were removed by centrifugation, the same buffer solution without nanotubes was added to the CdSe solution, and then the changes of PL were recorded.

5.8 Assembly and characterization of CNTs and QDs through DNA hybridization (Scheme 3, System 1)
The methodology of DNA detection by fluorescence measurement is shown in System 1. Two microliters of target oligonucleotide with different concentrations were added into the mixture of CNT-DNA (50 μL, [CNT]) 1 mg/mL, [DNA]) 0.1 nM) and QD-DNA probes (50 μL, [DNA]) 0.1 nM). This was mixed and incubated at 75 °C for 5 min and then at 25 °C for 20 min. After hybridization with target DNA, CNT-QD assemblies were formed and then removed by centrifugation at 2000 rpm for 5 min. The unbound QD-DNA probes in supernatant PBS buffer were immediately detected by spectrofluorometer. The wavelength λ = 480 nm of the laser source was used for the excitation of the CNT-QD detection system. The fluorescence signal was recorded over a range from λ = 450 nm to λ = 700 nm. NoncDNA target (CGC GAT CTC AGG TCG ATA GG) was used as the control experiment.

5.9 Three-component CNT-QD system with the purpose of detecting three different DNA targets simultaneously (Scheme 3, System 2)
Three QDs with different emission wavelengths at 510, 555, and 600 nm were used to simultaneously detect three target DNA molecules, as shown in System 2, called QD$_{510}$, QD$_{555}$, and QD$_{600}$ probes, respectively. There are six probes in this system: three CNT-DNA
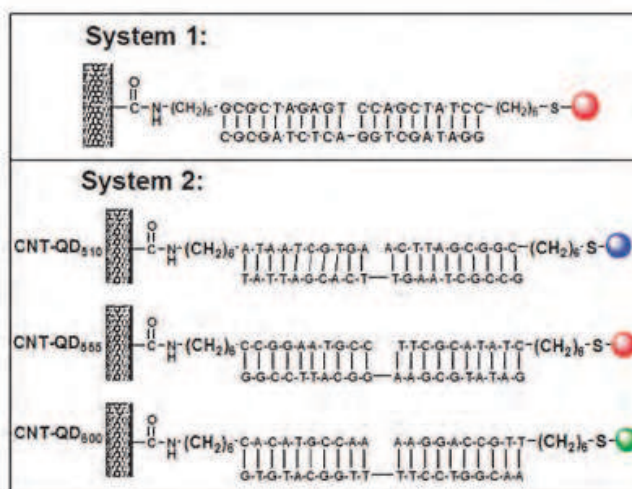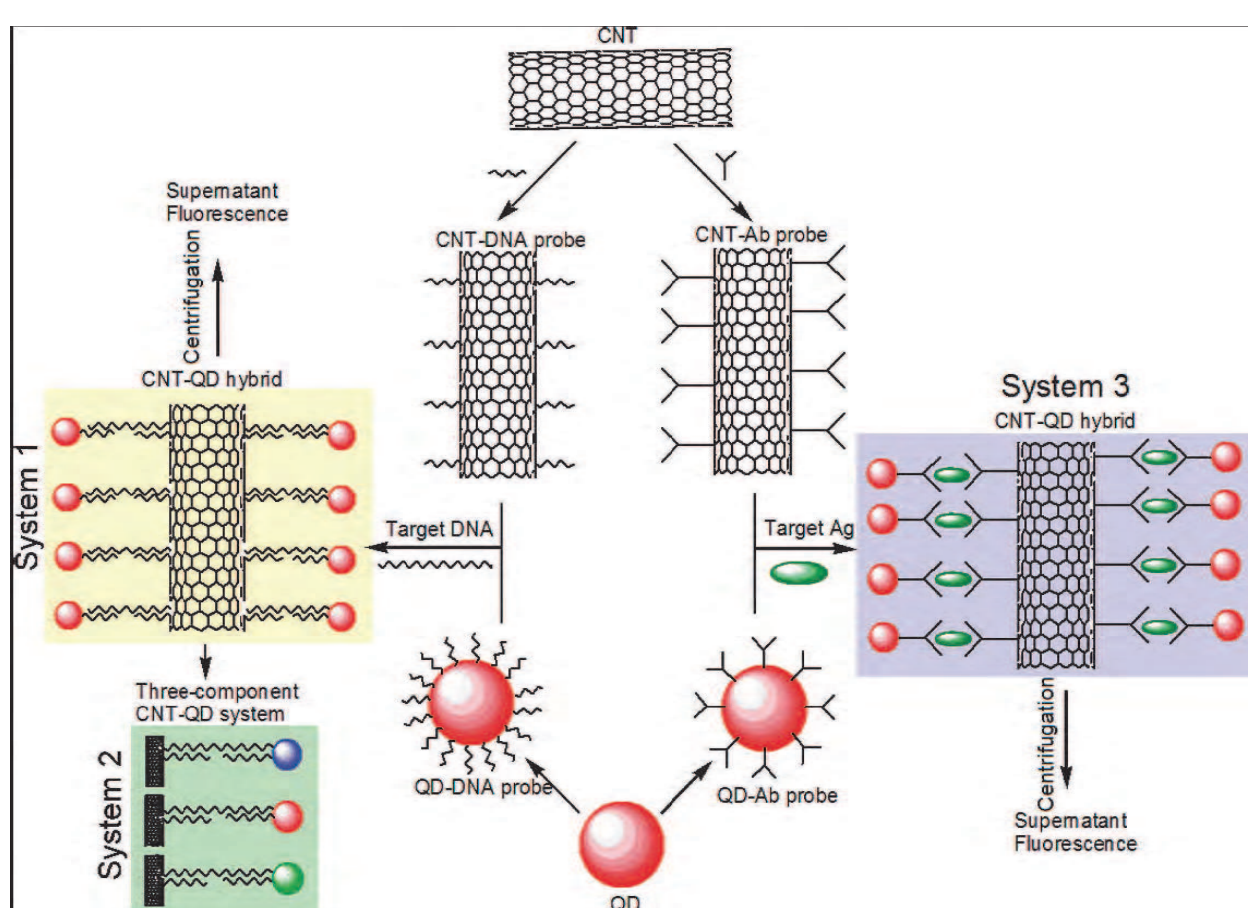
Scheme 3. Surface Functionalization of CNT (or QD) with Oligonucleotide/Antibody (Ab), Forming aCNT-DNA (or -Ab) Probe and QD-DNA (or -Ab) Probe, and Subsequent Addition of Target Oligonucleotide (or Antigen) to Form a CNT-QD Assembly^a (a The unbound QD probe was obtained by simple centrifugation separation, and the supernatant fluorescence intensity of QDs was monitored by spectrofluorometer. (System 1) Formation of CNT-QD hybrid in the presence of complementary DNA target. (System 2) Three-component CNT-QD system with the purpose to detect three different DNA targets simultaneously. (System 3) CNT-QD protein detection system based on antigen-antibody immunoreaction.) (With permission from American Chemical Society)

Simultaneous Detection of multi-DNAs and Antigens
Based on Self-Assembly of Quantum Dots and Carbon Nanotubes
257

probes (50 µL of each, [CNT]) 1 mg/mL and [DNA]) 0.1 nM) and 3 QD-DNA probes (50 µL of each, [DNA]) 0.1 nM) (as shown in Scheme 3, System 2). A mix of the six probes formed a uniform solution. Three cDNA targets were used in this system. Two microliters of each DNA target with different concentration was added into the six-probe mixture, individually. NoncDNA target (CGC GAT CTC AGG TCG ATA GG) was used as the control experiment. In addition, we mixed the three DNA targets (2 µL of each) to form a 6 µL DNA solution containing three different DNA targets, and then incubated the three DNA targets with the six-probe mixture simultaneously. The mixture solution containing probes and targets was incubated at 75 °C for 5 min and then at 25 °C for 20 min. After hybridization with target DNA molecules, CNT-QD assemblies were formed and then removed by centrifugation at 2000 rpm for 5 min. The unbound QD-DNA probes in supernatant PBS buffer were immediately detected by spectrofluorometer.
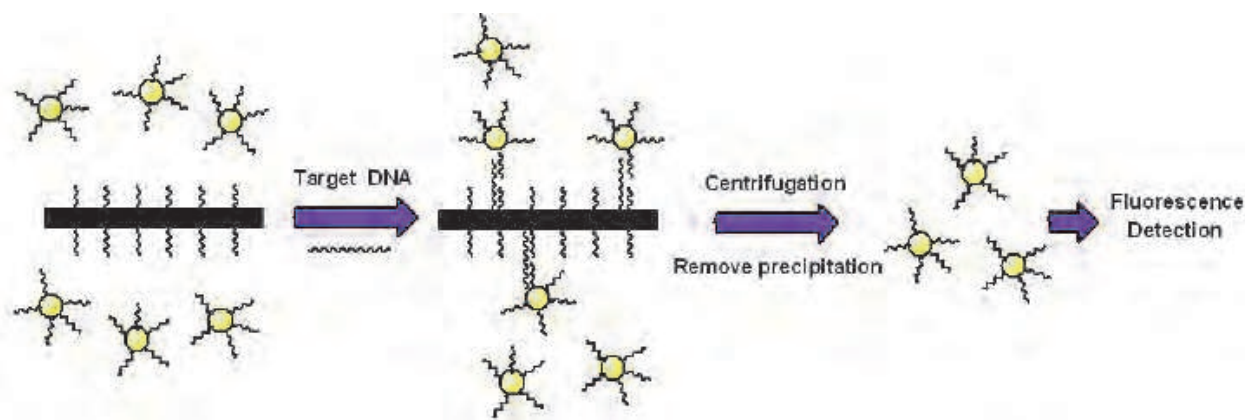
Scheme 4. Formation of CNT-QD assemblies for ultrasensitive DNA detection. (With permission from American Chemical Society)

5.10 CNT-QD system for antigen detection via antigenantibody immunoreaction (Scheme 3, System 3)

To confirm that the CNT-QD system can be used for antigen detection, a novel CNT-QD immunoassay system based on antigen-antibody immunoreaction was established. BRCAA1 protein was chosen as a typical example. CNT-Ab and QD-Ab probes were prepared as shown in the Supporting Information. The immunoreactions procedure is described as follows: 50 µL of CNT-Ab probe ([CNT]) 1.0 mg/mL, [Ab]) 1.0 nM) was reacted with 10 µL of BRCAA1 antigen (concentration from 0 to 1.0 nM) for 30 min, then 50 µL of QD-Ab probe (1.0 nM) was added, and the mixture was incubated for 2 h at room temperature. After the immunoreaction, the sandwich-type immunocomplex was formed on the surface of CNT probes. The unbound QDs-pAb was obtained by simple centrifugation separation and the supernatant fluorescence intensity of QDs was monitored by spectrofluorometer (Scheme 4.).

5.11 Characterization of CNT-QD hybrids

TEM images were taken with a JEM 100-CXII microscope (JEOL, Japan) at 100 kV to demonstrate the formation of CNT-QD assembly. The zeta potentials of CNT-QD aqueous suspension were measured using a MALVERN ZETAZIZER 2000 instrument (U.K.). Fourier

transform infrared (FT-IR) spectra were recorded using a PE Paragon 1000 spectrometer. UV–vis absorption spectra were obtained on UNICAM UV 300 spectrometers (Thermo Electronic). Raman measurements were carried out on a Jobin Yvon microRaman system (Ramanor U1000, Instruments SA, USA) using a Spectra-Physics Ar ion laser at an excitation wavelength of 514.5 nm (2.41 eV). All measurements were taken at room temperature, and for each sample the Raman data were collected at different light spots on the sample surface. For every Raman spectrum taken, the position of the peaks was verified by calibrating the spectral positions with respect to the silicon substrate peak seen at 521 cm^{-1}.

6. Results and discussion

6.1 Formation of self-assembled CNT-QD nanocomplex

TEM images of QDs, CNTs, and CNT-QD nanocomplexes are shown in Fig. 11. The size distribution of CdSe nanoparticles is narrow with an average particle size of 3.0 nm in diameter, while the diameters of CNTs are about 20~30 nm. When the colloids of CdSe nanoparticles were mixed with CNT-COOHs or CNT-OHs in aqueous solution, very few CdSe nanoparticles can be bound onto the nanotubes (Fig. 11a, b). On the other hand, the TEM images give a direct view of the CdSe nanoparticles binding to CNT-NH$_2$ (Fig. 11c); the CNTs with -NH$_2$ surface groups are densely coated with CdSe nanoparticles. For all three CNT/QD systems no precipitation was observed for at least 4 weeks. For CNT-COOH, most of the CNTs remained suspended for over 1 year after adding CdSe QDs because of the strong electrostatic repulsion between CNTs and QDs, which is consistent with the TEM pictures as shown in Fig. 11.
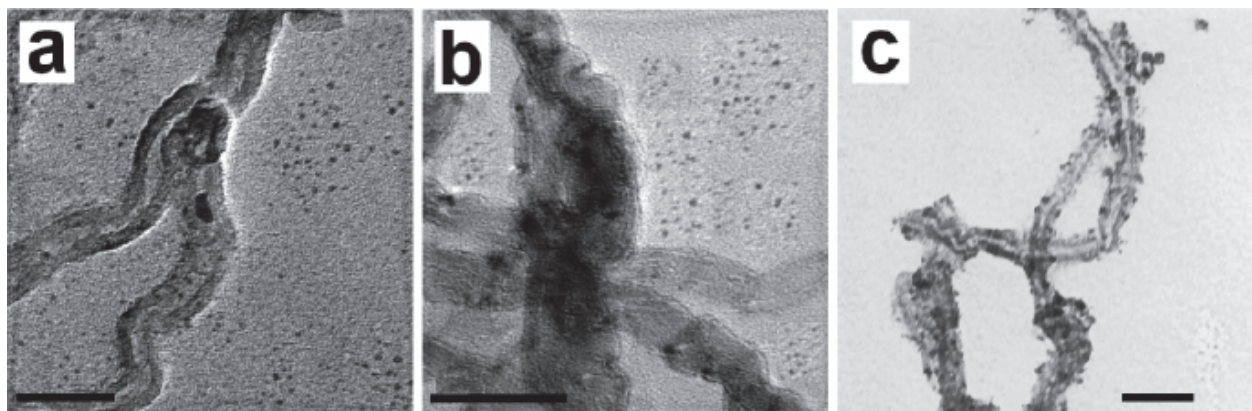

Fig. 11. TEM images of (a) a mixture of CNT-COOH and CdSe, (b) a mixture of CNT-OH and CdSe, and (c) self-assembled CNT-NH$_2$-CdSe nanocomplexes. Scales bar: 50 nm. (With permission from American Chemical Society)

To further investigate the interaction between CNTs and QDs, the ζ-potential of the CNTs and CdSe samples are summarized in Fig. 12. Positively charged CNT-NH$_2$, negatively charged CNT-COOH, and negatively charged QD-COOH can be confirmed from ζ-potential analysis. Thus, addition of positively charged –NH$_2$-modified CNTs to the negatively charged CdSe QDs with a COOH group results in formation of CNT-CdSe complexes by electrostatic interaction as shown in Scheme 1. The interaction forces between QDs and CNTs in aqueous solution are mainly electrostatic forces, which is why they are weakest for negative carboxyl-terminated CNTs. At pH 7.0, CdSe has a negative charge (ζ potential = 36

mV from Fig. 12); therefore, amino-terminated cationic CNTs (ζ potential = +32 mV) have the biggest impact on the QDs.

The UV-vis absorption spectra of CdSe nanocrystals (a) before adding CNT solution and (b) after adding CNT-COOH, (c) CNT-OH, and (d) CNT-NH$_2$ are shown in Fig. 13A. The spectral feature located at ca. 580 nm has been assigned to the first excitonic transition occurring in CdSe nanocrystals. No obvious change of the band gap (580 nm) of the QDs is observed after adding CNT samples, indicating that no larger QD agglomerates were formed after adding CNT; in particular, for the CNT-NH$_2$-QD samples, individual QD was separately coated on the CNT surface (Fig. 11c) instead of agglomerate.
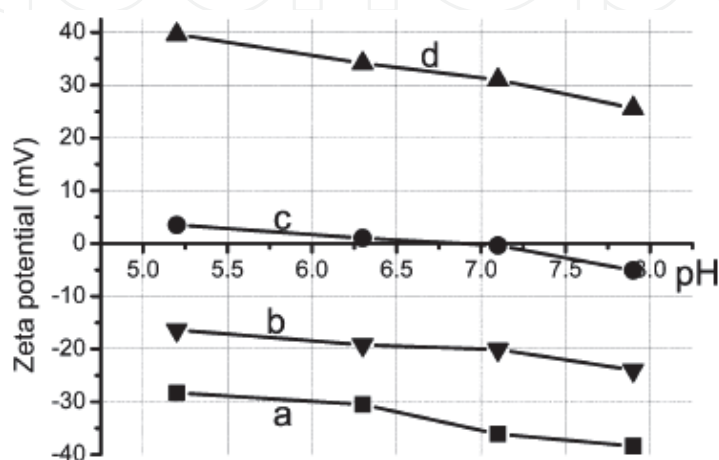

Fig. 12. Zeta potentials of (a) mercaptoacetic acid coated CdSe, (b) CNT-COOH, (c) CNT-OH, and (d) CNT-NH$_2$ in aqueous solution. (With permission from American Chemical Society)

6.2 Photoluminescence (PL) quenching of CdSe QDs in the presence of CNTs

The PL emission spectra (Fig. 13B-D) show that CdSe QDs have strong PL, and the wavelength of the PL maximum for CdSe was at 552 nm. The CNT concentration dependence of the PL intensity of CdSe QDs is shown in Fig. 13B-D. The decrease in the PL intensity was the most marked change in the PL spectrum observed upon addition of CNTs. For all types of CNTs, their increasing concentrations caused a linear reduction in the PL of CdSe. The effect was strongest for CNT-NH$_2$ (Fig. 13D), less pronounced for CNT-OH (Fig. 13C), and weakest for CNT-COOH (Fig. 13B).

6.3 Calculation of quenching constants from the Stern-Volmer equation and double-logarithmic equation

The PL quenching data were analyzed by the Stern-Volmer equation (Fan and Jones Jr, 2006; Maurel et al., 2006; Pan et al., 2006c) :

$$\frac{I_0}{I} = 1 + K_{SV}\left[CNT\right] \tag{1}$$

where I_0 and I are, respectively, PL intensities in the absence and presence of CNT, K_{SV} is the Stern-Volmer dynamic quenching constant, and [CNT] is the concentration of CNT. The equation assumes a linear plot of I_0/I versus [CNT], and the slope is equal to K_{SV}. The Stern-

Volmer constants express CdSe QD accessibility to the CNT. Fig. 14A shows Stern-Volmer quenching curves describing I_0/I as a function of CNT concentration. The Stern-Volmer constants (K_{SV}) for quenching of CdSe PL intensity by different kinds of CNTs are presented in Table 1. K_{SV} were calculated from the plots shown in Fig. 14A.
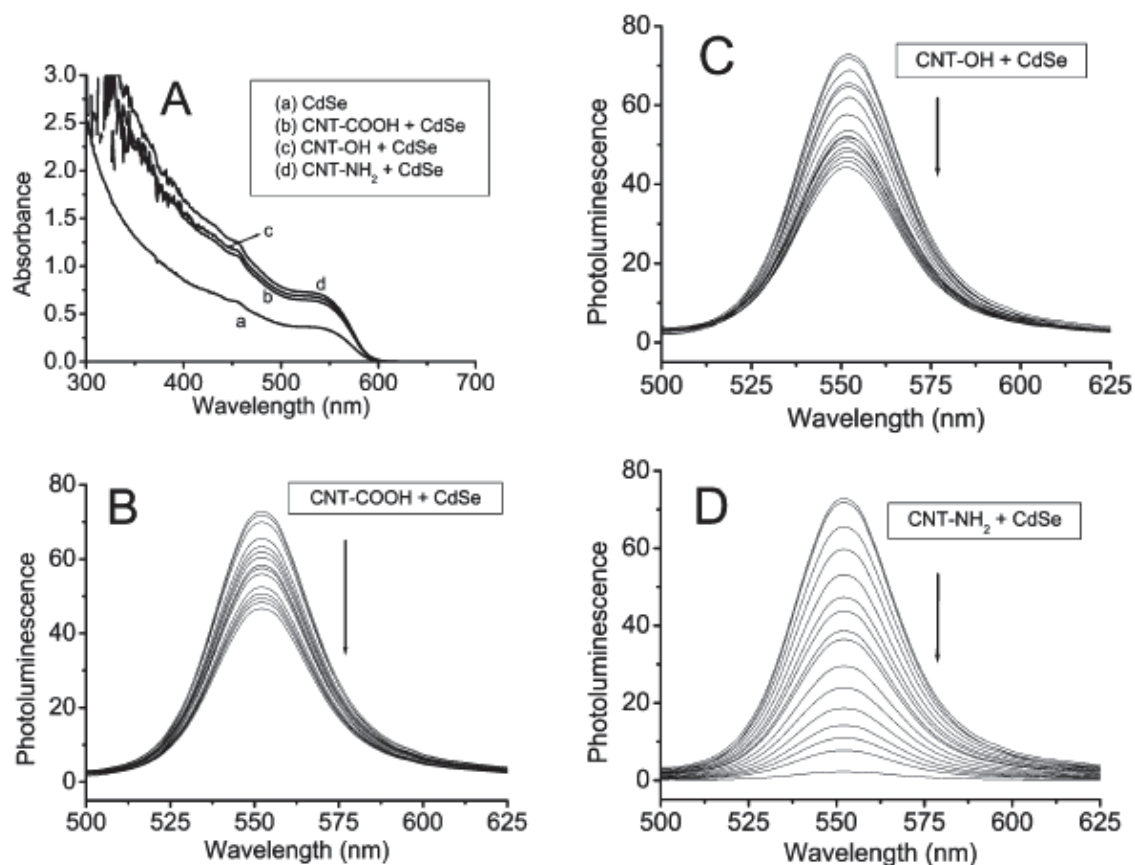

Fig. 13. (A) UV-vis spectra of QDs before and after adding CNTs; (B-D) PL spectra of CdSe QDs by adding CNTs. The concentration of CNT from top to bottom: 0, 0.5, 1.0, 2.0, 3.0, 4.0, 5.0, 6.0, 7.0, 8.0, 9.0, 10.0, 20.0, 30.0, 50.0, and 100.0 (mg/L). (With permission from American Chemical Society)

6.3 Calculation of quenching constants from the Stern-Volmer equation and double-logarithmic equation

The PL quenching data were analyzed by the Stern-Volmer equation (Fan and Jones Jr, 2006; Maurel et al., 2006; Pan et al., 2006c) :

$$\frac{I_0}{I} = 1 + K_{SV}[CNT] \tag{1}$$

where I_0 and I are, respectively, PL intensities in the absence and presence of CNT, K_{SV} is the Stern-Volmer dynamic quenching constant, and [CNT] is the concentration of CNT. The equation assumes a linear plot of I_0/I versus [CNT], and the slope is equal to K_{SV}. The Stern-Volmer constants express CdSe QD accessibility to the CNT. Fig. 14A shows Stern-Volmer quenching curves describing I_0/I as a function of CNT concentration. The Stern-Volmer

Simultaneous Detection of multi-DNAs and Antigens
Based on Self-Assembly of Quantum Dots and Carbon Nanotubes
261

constants (K_{SV}) for quenching of CdSe PL intensity by different kinds of CNTs are presented in Table 1. K_{SV} were calculated from the plots shown in Fig. 14A.
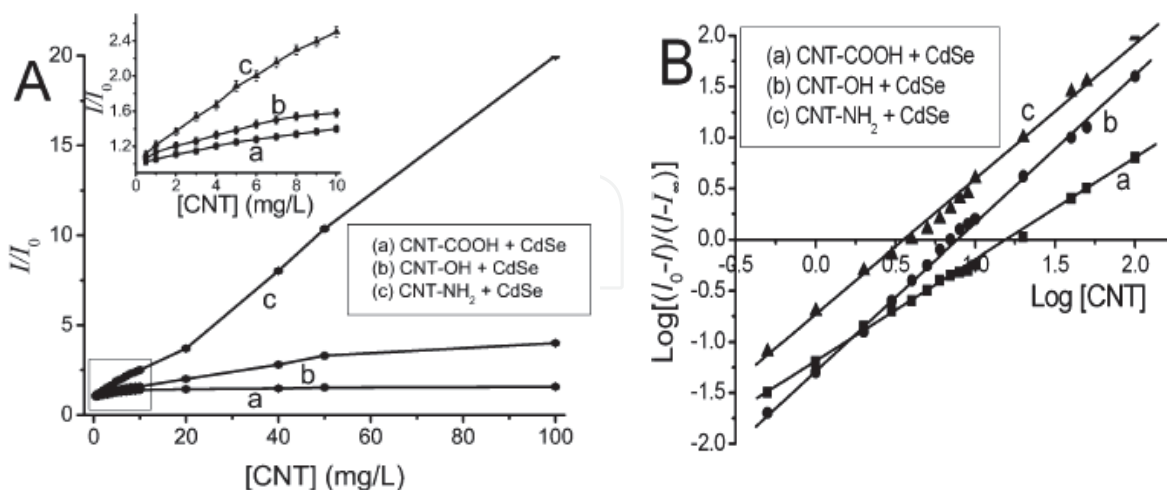

Fig. 14. (A) Stern-Volmer plot and (B) double-logarithmic plot for CdSe PL quenching by CNT with different concentration. (With permission from American Chemical Society)

Alternatively, analyses of the PL data were performed using the double-logarithmic equation (Pan et al., 2006c). According to this approach, the QDs PL intensity scales with the CNT concentration ([CNT]) through the following equation:

$$\frac{I_0 - I}{I - I_s} = \left[\frac{CNT}{K_{diss}} \right]^n \tag{2}$$

The binding constant K_b is obtained by plotting $\log[(I_0 - I)/ (I - I_s)]$ versus $\log[CNT]$, where I_0 and I_s are the PL intensities of the QDs alone and the QDs saturated with the CNTs, respectively. The slope of the double-logarithm plot obtained from the experimental data is the number of n, whereas the value of $\log[CNT]$ at $\log[(I_0 - I)/ (I - I_s)]) 0$ equals the logarithm of the dissociation constant K_{diss}. The reciprocal of K_{diss} is the quenching constant Kb. The PL intensity values (I) were obtained from the area under the PL spectra. Figure 4B represents the plot of $\log[(I_0 - I)/ (I - I_s)]$ versus $\log[CNT]$ for CNT-COOH, CNT-OH, and CNT-NH$_2$. Values of K_b and n obtained from Fig.14B are shown in Table 1.

sample	Stern-Volmer equation K_{SV} [L/mg]	Double-logarithmic equation K_b (n) [L/mg]
CNT-COOH	0.060	0.0631(1.000)
CNT-OH	0.106	0.1365(1.434)
CNT-NH$_2$	0.176	0.269(1.346)

Table 1. Quenching Constants of CdSe by CNTs from the Stern-Volmer Equation and Double-Logarithmic Equation.

PL of CdSe QDs was strongly quenched by amino-terminated CNTs but only poorly quenched by CNT-COOH, as shown by K_{SV} and K_b values. The data were well fitted by a straight line, typical of a simple dynamic quenching mechanism. For [CNT] >10 mg/L, KSV values increase rapidly for CNT-NH$_2$ + QD solution, but fewer changes can be observed for

CNT-OH + QD and CNT-COOH + QD solution. The data shown in Table 1 indicate that quenching constants of K_{SV} and K_b from the Stern-Volmer equation and double-logarithmic equation are very similar. The quenching constant (K_{SV} and K_b) for CNT-NH$_2$ is much higher than that of CNT-COOH and CNT-OH, indicating CNT-NH$_2$ is more strongly bound to the QD compared with CNT-COOH and CNT-OH. These observations support that surface groups and their charges are key factors of the CdSe-CNT interactions, which also confirm that PL properties of CdSe QDs are closely associated with their surface structure and surface charges. The ζ-potential analysis in Fig. 12 showed that both carboxyl and amino surface groups are ionized in water, only hydroxyl-terminated CNTs bear no charge on their surface. Thus, the dynamic process quenched the emission of CdSe QDs because of the electrostatic interactions between the CNT surface and CdSe surface in aqueous solution.

From the results of TEM, zeta-potential analysis, PL quenching experiments, the Stern-Volmer equation, and the doublelogarithmic equation we can make conclusions that the quenching intensity of CdSe caused by CNT highly depends on the surface structure and charge of CNTs and can be ordered as follows: CNT-NH$_2$ > CNT-OH > CNT-COOH.

6.4 Effect of pH on the quenching constants

Control experiments were carried out by adding the same buffer but without CNTs to QD solution; furthermore, buffer samples with pH ranging from 4.0 to 10.4 were used to investigate the pH effect on QD PL properties. As shown in Fig. 15A, little PL change can be observed for QDs after adding buffer solutions without CNT at pH values from 4.0 to 10.4, which highly suggest that PL quenching was mainly caused by the CNTs in the QD solution.
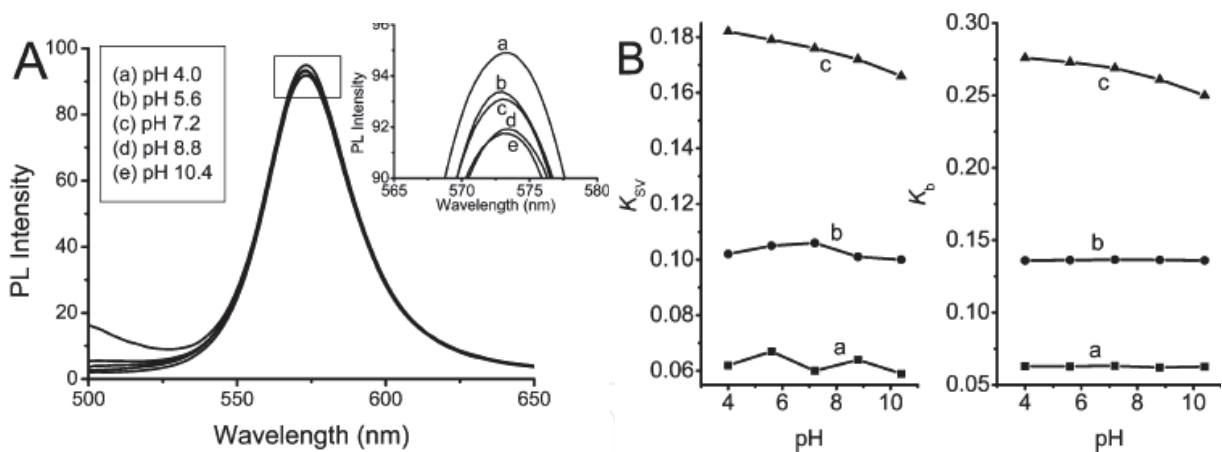

Fig. 15. (A) pH effect of buffer solution on QD PL intensity. (B) Plot of quenching constant versus solution pH: (a) CNT-COOH, (b) CNT-OH, and (c) CNT-NH$_2$. (With permission from American Chemical Society)

To investigate the pH effect on quenching constant (K_{SV} and K_b), CNTs were added to QD solution at different pH environments, and then K_{SV} and K_b were calculated from the Stern-Volmer equation and double-logarithmic equation. Plots of quenching constant versus pH value are given in Fig. 15B. In the CNT-NH$_2$ case, the quenching constant (K_{SV} and K_b) values decreased slightly with increasing pH from 4.0 to 10.4. It can be explained as follows. QD is negatively charged by the zeta potential result (Fig. 12). At lower pH, amino groups of CNT-NH$_2$ are highly protonated, but at higher pH, the surface charge becomes less positive; thus, the electrostatic interactions between amino groups CNT-NH$_2$

and the QD molecule are weakened, resulting in the decrease of quenching constants. For CNT-COOH and CNT-OH samples, little changes in K_{SV} and K_b can be observed as shown in Fig. 15B.

6.5 FT-IR and raman spectroscopy

As shown in Fig. 16A (a), the FT-IR spectrum of the carboxylic-acid-coated QDs showed a strong asymmetric vibration characteristic of carboxyl groups at 1711 cm^{-1}. The FT-IR spectra of QDs after adding CNT-COOH and CNT-OH are shown as Fig. 16A (b, c), indicating no shift of the -COOH peak at 1711 cm^{-1}. The QD-COOH peak at 1711 cm^{-1} shifts to 1732 cm^{-1} after adding CNT-NH$_2$, indicating a strong electrostatic interaction between CNT-NH$_2$ and QDs. Raman spectra of CNT-NH$_2$ before and after binding with QDs are shown in Fig. 16B. CNT-NH$_2$ reveals two main peaks at 214 and 1582 cm^{-1} in the Raman spectrum. After attachment of QDs onto the sidewalls of CNT-NH$_2$, the original G peak at 1582 cm^{-1} of the uncoated CNT-NH$_2$ was shifted to 1578 cm^{-1} (Fig. 16B). However, adsorption of QD on CNT-NH$_2$ did not result in any Raman shift at 214 cm^{-1}, indicating that the assembly of QD nanocrystals onto the tubes deformed the sidewall of CNTs (Pan et al., 2006b). For CNT-COOH and CNT-OH, no Raman shift can be observed after addition of QDs (data not shown), indicating CNT-QD complexes cannot be formed by adding QD to the CNT-COOH or CNT-OH.
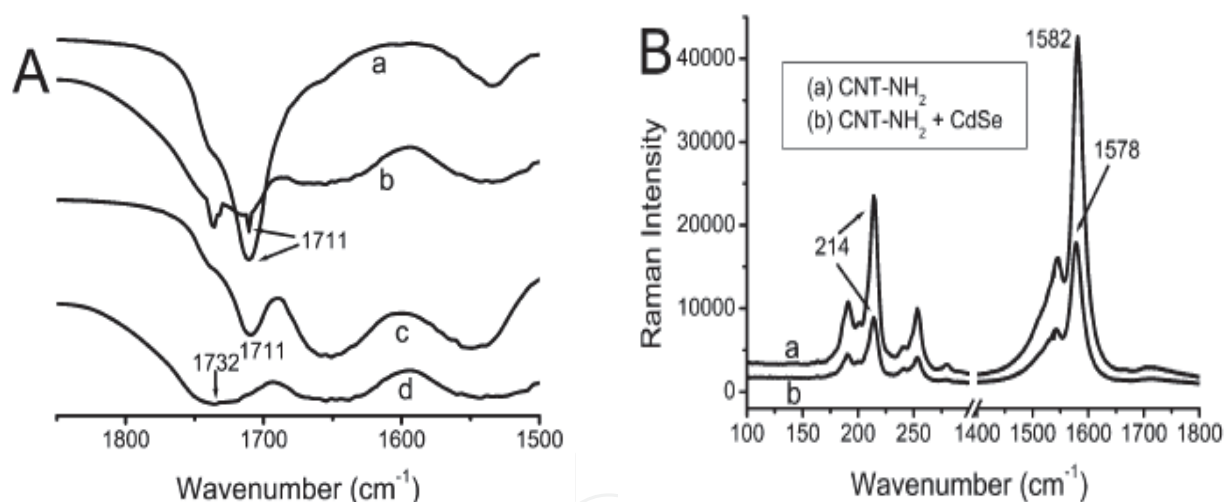

Fig. 16. (A) FT-IR spectra of (a) QD-COOH, (b) CNT-COOH + QD, (c) CNT-OH + QD, and (d) CNT-NH$_2$ + QD. (B) Raman spectra of CNT-NH$_2$ and CNT-NH$_2$ + QDs. (With permission from American Chemical Society)

6.6 The quenching mechanism between CdSe QDs and CNTs

With the linearity, the concentration of CNT can be monitored by measuring the PL intensity of CdSe QDs. PL quenching is a process which decreases the intensity of the QD PL emission. QD PL quenching may occur by several mechanisms (Fan and Jones Jr, 2006; Pan et al., 2006c): (1) dynamic quenching, (2) static quenching, (3) quenching by energy transfer, and (4) charge-transfer reactions. In this paper we can draw the conclusion that QD quenching in the presence of CNTs is mainly caused by dynamic quenching and energy-transfer mechanisms (Clapp et al., 2004; Oh et al., 2005). When quenching occurs by a dynamic mechanism, the quenching is an additional process that deactivates the

excited state besides radiative emission (Cui et al., 2004b). The dependence of the QD emission intensity on CNT concentration is given by the Stern-Volmer equation and double-logarithmic equation. The accessibility of CNT to QD is reflected in the quenching constant (including K_{SV} and K_b). For CNT-COOH and CNT-OH, low values of K_{SV} and K_b indicate low exposure of CdSe to CNTs, i.e., the QD did not attach to the CNT surface. In particular, in the case of CNT-COOH, strong repulsion between CNT and QD in aqueous solution can be confirmed by the TEM image and zeta-potential data. The interparticle space between CNT and QD will be the main determinative factor for PL quenching according to the dynamic quenching and energy transfer mechanisms. According to energy-transfer mechanism, energy transfer is proportional to r^{-6} (r = distance between CNT and QD), i.e., PL will be severely quenched when QDs are getting close to the surface of the CNT. It is very difficult for QD-COOH to reach the CNT-COOH surface because of the strong repulsion electrostatic force. However, QD-COOH can easily bind to the CNT-NH$_2$ surface to form CNT-QD nanocomplex, which can be confirmed by FT-IR and Raman spectroscopy, resulting in strong PL quenching of QDs; thus, the strong quenching of QDs caused by CNT-NH$_2$ is mainly due to attachment of the QDs onto the CNT surface. These QDs have no shifted emissions at 552 nm (Fig. 13), indicating a relatively unchangeable size. Given that the CNTs quenched the CdSe QDs, the interaction between CNTs and QDs must provide an alternative, nonirradiative decay path (Clapp et al., 2004; Cui et al., 2004b; Oh et al., 2005). It is believed that this nonirradiative decay path occurs because the electron affinity between the CdSe QDs and the CNTs is sufficiently different that it allows electron transfer from the QDs to the CNTs (Clapp et al., 2004; Pan et al., 2006c). In other words, formation of CNT-QD conjugates favors electron transfer from the quantum dots (donor) to the CNTs (acceptor) such that the excited electrons are accepted by the CNTs rather than being emitted as the PL peak. For CNT-COOH and CNT-OH, QDs cannot reach the CNTs surface, so that energy transfer will be very difficult to occur for the CNT-COOH/QD or CNT-OH/QD system; therefore, a dynamic quenching mechanism will be fit for the CNT-COOH/QD or CNT-OH/QD system. For CNT-NH$_2$/QD system, besides dynamic quenching, electron/energy transfer will be allowed from QDs to CNTs, i.e., an energy-transfer quenching mechanism.

6.7 CNT-QD assembly system for DNA target detection (System 1)

The supernatant fluorescence spectra in Fig. 17 show that the QD-DNA probe has strong fluorescence, and the maximum fluorescence wavelength for CdSe was at ~570 nm. The cDNA target (sequence shown in Scheme 3, system 1) with concentration ranges of 0~200 pM was added to the mixture of CNT-DNA and QD-DNA probes to form CNT-QD nanohybrids. After centrifugation at 2000 rpm for 5 min, the CNT-QD nanohybrids were removed; therefore, only unbounded QD-DNA existed in the supernatant buffer. The decrease in the fluorescence intensity was the most marked change in the fluorescence spectrum observed upon addition of the cDNA target.

Control experiments were carried out by adding cDNA target to the QD-DNA solution in the absence of the CNT-DNA probe (Fig.18A). In addition, buffer solutions with pH ranging from 4.0 to 11.0 were used to investigate the pH effect on the fluorescence properties of the QD-DNA probe (Fig.18B). As shown in Figure 2A and B, little PL change can be observed for QD-DNA probes after adding complementary target DNA solutions without CNT-DNA probe at pH values from 4.0 to 11.0, which highly suggests that the QD fluorescence intensity was
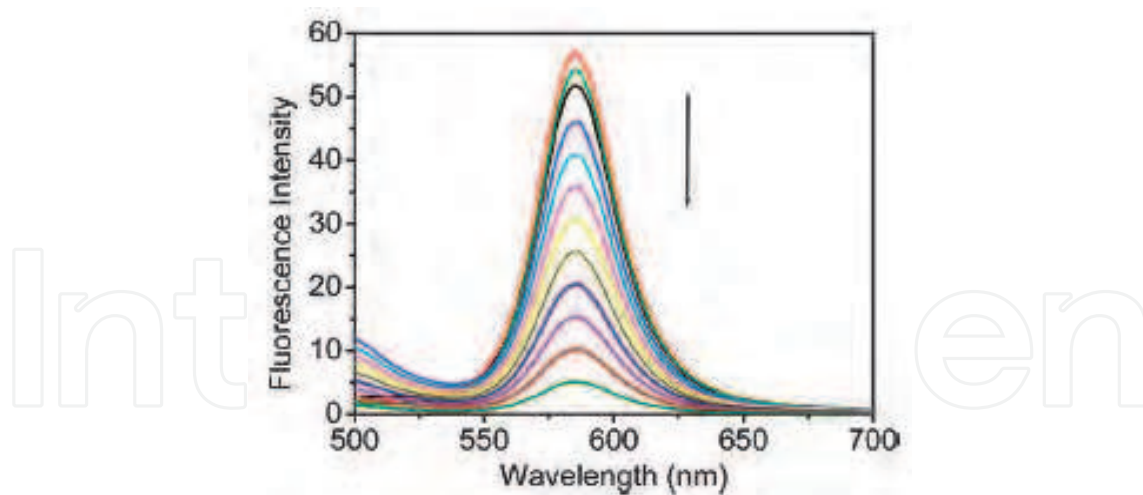
Fig. 17. Fluorescence intensity of supernatant after adding target 1 with different concentrations (from top to bottom): 0, 10, 16, 25, 40, 50, 60, 75, 90, 120, 150, and 200 pM. (With permission from American Chemical Society)
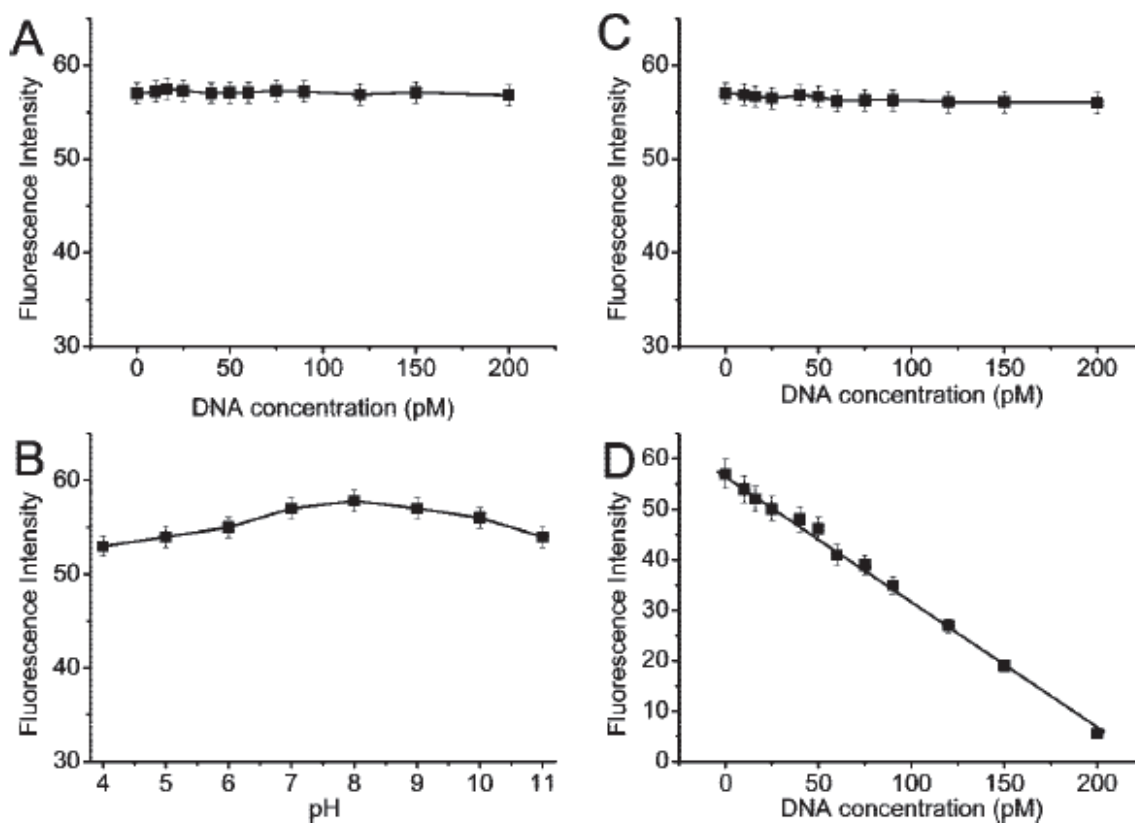

Fig. 18. Plot of supernatant fluorescence intensity versus DNA concentration: (A) effect of cDNA target concentration on fluorescence intensity of QD-DNA probe; (B) fluorescence of QD-DNA probe at different pH values from 4.0 to 11.0; (C) noncDNA target with concentration from 0 to 200 pM incubated with CNT-DNA and QD-DNA probes (no fluorescence changes in supernatant); and (D) marked fluorescence decrease found for CNT-DNA/QD-DNA mixture solution after the incubation with cDNA target. (With permission from American Chemical Society)

stable in the presence of oligonucleotides at different pH values. From the plot of fluorescence intensity versus DNA concentration (Fig. 18D), their increasing concentrations caused a linear reduction in the fluorescence intensity of QDs at the target 1 concentration range of 0~200 pM. Furthermore, noncDNA target was used as a control, and after addition of noncDNA target, little fluorescence change can be observed (Fig. 18C), indicating no CNT-QD assembly can be formed in the presence of noncDNA . In this experiment, the available DNA detection range is from 0 to 200 pM, and according to the measurement results on the samples of gradually diluted DNA targets, the available good repeatability limit of detection is as low as ~0.2 pM (Fig. 18D).

6.8 Simultaneous three DNA target detection based on CNT-QD assembly system (System 2)

Three QDs with different emission wavelengths at 510, 555, and 600 nm were used as probes to detect three target DNA molecules simultaneously (called QD_{510}, QD_{555}, and QD_{600} probes). Their spectrally resolved fluorescence signal is displayed in Fig. 19A. As can be seen, the fluorescence signal can be split into three bands with emission wavelengths of 510 (QD_{510}), 555 (QD_{555}), and 600 nm (QD_{600}). Plotting the fluorescence intensities for the three wavelengths, that is, $\lambda = 510$, $\lambda = 555$, and $\lambda = 600$ nm, respectively, against the concentration of DNA targets results in the linear decrease of fluorescence intensity given in Fig. 19B-F. In Fig. 19B, we used a noncDNA target as control experiment, no fluorescence changes of the supernatant after incubation of noncDNA can be observed, indicating no CNT-QD hybrid formation in this system. By adding three cDNA targets all together to the CNT-DNA and QD-DNA probe solution (six-probe solution), we found a fluorescence decrease at the three wavelengths (510, 555, and 600 nm; Figure 19C), indicating CNT-QD hybrids formed in all the probes corresponding to three different wavelengths. In Figure 19D, only one cDNA target (sequence shown in Scheme 3, system 2, CNT-QD_{510}) was incubated with the six-probe solution, and we found fluorescence decreased only at 510 nm, and no fluorescence changes were found at 555 and 600 nm, indicating there is only CNT-QD_{510} hybrid formed, but no CNT-QD_{555} and CNT-QD_{600} hybrids. Similar results can be seen from Fig. 19E and F. Only CNT-QD_{555} and CNT-QD_{600} hybrids were formed upon the addition of only corresponding cDNA target, respectively. Briefly, we demonstrated the CNT-QD system can be used as simultaneous multicomponent detection system with detection limits of ~0.2 pM for each DNA target.

From Fig. 19C-F and Fig. 18D, we noticed that fluorescence intensity is 60 at [DNA] = 0, but on the other hand, fluorescence intensity was 0 at [DNA] = 225 pM. Although at the fluorescence intensity= 0, the amount of target DNA is 2 μL × 225 pM = 4.5×10^{-16} mol. In the CNT-DNA probe and QD-DNA solution, [DNA] = 1.0 nM and volume = 50 μL, so the DNA amount in the CNT-DNA probe or QD-DNA probe solution is 50 μL × 0.1 nM = 5×10^{-15} mol. From Figure 18D, if we assumed all QD particles were binding to the CNT surface at the point of fluorescence intensity = 0, we concluded that the QD number should be equal to the DNA amount (i.e., 4.5×10^{-16}), so the number of DNA molecules on each QD particle is: 5×10^{-15} mol/4.5×10^{-16} = 11. That is to say, there are 11 DNA molecules on each QD, and only 1 DNA molecule performed DNA hybridization to produce the CNT-QD hybrid. But we could not calculate the number of DNA probes on each CNT, since the lengths of the CNT were not known.
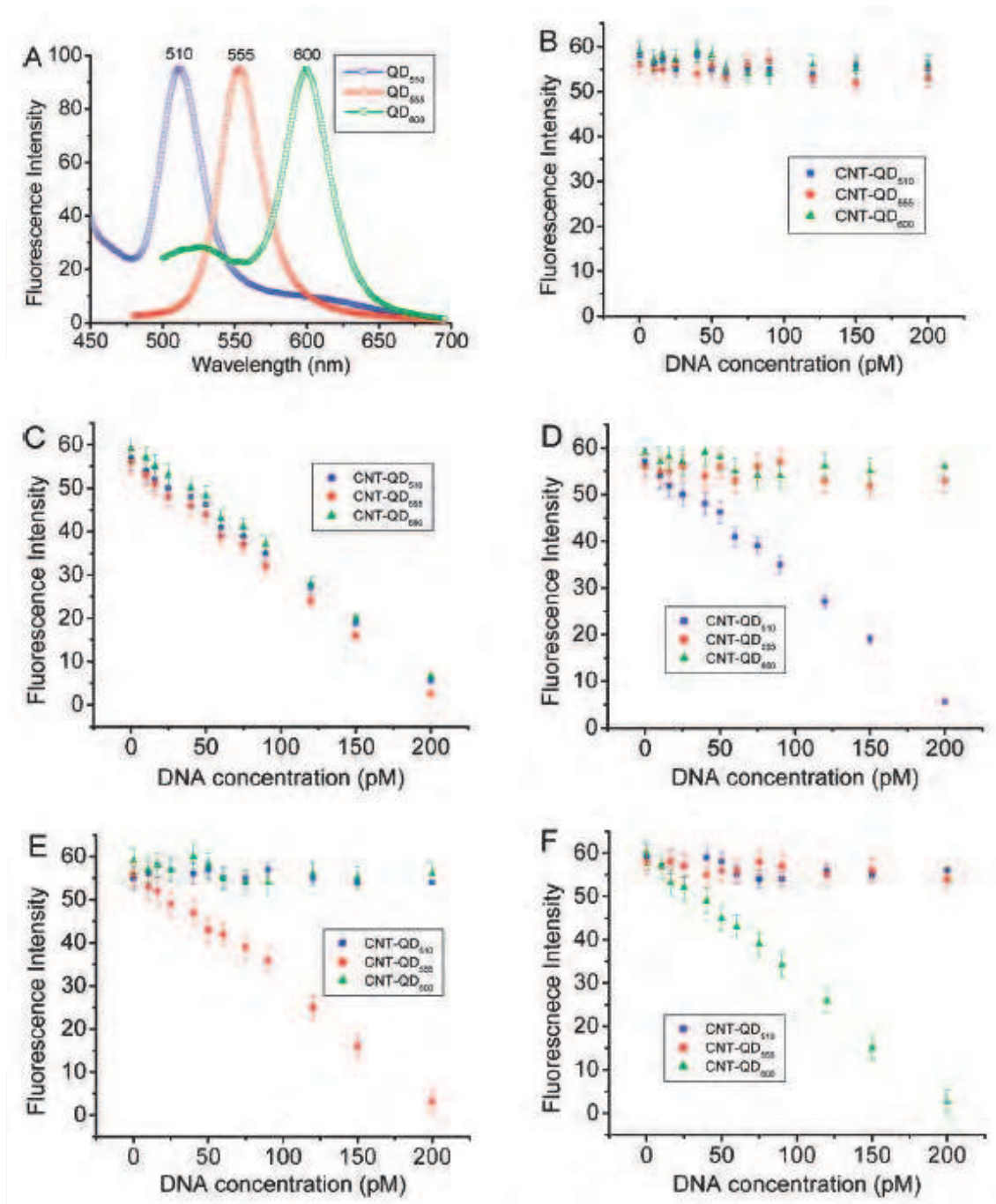
Fig. 19. Sensitivity and linearity analysis of the three-component CNT-QD DNA detection system by plotting fluorescence intensity against target DNA concentration. (A) QD probes with three different fluorescence wavelengths at 510, 555, and 600 nm; (B) plotting of supernatant fluorescence intensity against DNA concentration upon incubation of noncDNA target with CNT-DNA and QD-DNA probes; (C) fluorescence decreased at the three peaks 510, 555, and 600 nm upon the adding three cDNA targets to the six-probe solution; (D) only the 510 nm band decreased by adding the only DNA target corresponding to CNT-QD510 system; and (E, F) fluorescence decreases at 555 and 600 when cDNA corresponding to CNT-QD$_{555}$ and CNT-QD$_{600}$ system, respectively, is added. (With permission from American Chemical Society)

According to Fig. 18D and Fig. 19C-F, the QD fluorescence intensity (F) scales with the DNA concentration [DNA] (pM) through the following:

$$F = -26.7 \, [DNA] + 60 \qquad (3)$$

6.9 CNT-QD assembly for antigen detection via antigen-antibody (Ag-Ab) immunoreaction (System 3)

The purpose of the CNT-QD assembly system is to ultrasensitively detect target biomolecules, trying to confirm that the CNT-QD ultrasensitive detection system can be used not only for a cDNA target, but also for an antigen-antibody system. The formation of the CNT-QD hybrid via immunoreaction of an antigen with CNT-Ab and QD-Ab probes can be demonstrated from the fluorescence decrease of unbound QD fluorescence, as shown in Fig. 20. Similar to System 1, we used the QD particles with fluorescence emission wavelength at 570 nm. Upon incubating with target BRCAA1 antigen, CNT-QD hybrid was removed by a simple centrifugation step, and supernatant QD fluorescence intensity decreased linearly at an antigen concentration ranging from 0 to 1.0 nM (Fig. 20a). By measuring the gradually diluted samples, we found that we can obtain good repeatability results within the concentration scope of more than ~0.01 nM, which is also located within the scope of linearity between the QDs fluorescence and BRCAA1 concentration. For the control experiment, in the absence of the target antigen, no fluorescence decrease was observed from Fig. 20b.
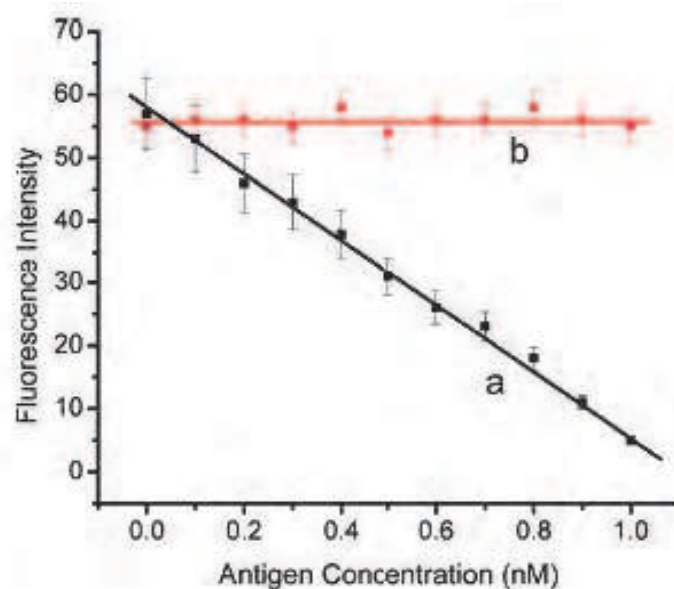

Fig. 20. CNT-QD assembly system for antigen detection. (a) Linear plot of fluorescence intensity in supernatant against antigen concentration and (b) control experiment were conducted in the absence target antigen. (With permission from American Chemical Society)

From Fig. 20, we noticed that the fluorescence intensity is 0 at the point of the target [Ag] = 1.1 nM; that is, the amount of antigen is 1.1 nM $\times$ 10 µL = 1.1×10^{-14} mol. In CNT-Ab and QD-Ab probes, the antibody amount is 1.0 nM $\times$ 50 µL = 5×10^{-14} mol. The antibody number on each QD particle is (5×10^{-14} mol) / (1.1×10^{-14} mol) = 4.5, so we concluded that 4.5 antibody molecules are on each QD particle, and only 1 antibody on QD bound to the antigen to form the CNT-QD hybrid.

Simultaneous Detection of multi-DNAs and Antigens
Based on Self-Assembly of Quantum Dots and Carbon Nanotubes
269

According to Fig. 20, the QD fluorescence intensity (F) scales with the antigen concentration [Ag] (nM) through the following:

$$F = -51.8 \, [Ag] + 57 \tag{4}$$

As a comparison, the ELISA detection method for BRCAA1 antigen was performed according to the testing procedure for antigen-antibody interaction. The novel CNT-QD hybrids method reported herein was compared with ELISA (Cui et al., 2004a; Medintz et al., 2005; Pan et al., 2006a). BRCAA1 antigen samples were especially selected to be used for the immunoassay using the ELISA methods, and the result was ~0.5 nM. In the case of protein detection, BRCAA1 antigen with a concentration < 0.5 nM cannot be detected by using the ELISA methods. In the CNT-QD method, BRCAA1 antigen can be detected with good repeatability at ~0.1 nM below the detection limit. The results suggest the excellent CNT-QD method has a higher sensitivity than ELISA. The protein detection limit is ~0.1 ppm by using a Dot-Blot fluorescent staining method (Yamada et al., 2004). In the case of oligonucleotide detection, the detection limit of the colorimetric polynucleotide detection method (Elghanian et al., 1997) is the same as that of our method. Bio-Barcodes assays have been studied and work comparably well over the 20~700 nM target concentration range (Nam et al., 2002; Nam et al., 2003). Therefore, quantification and detection of DNA/protein can be performed with higher accuracy and sensitivity.

Regarding the potential mechanism, the CNT probe and QD probe can form the nanocomposites under the existence of the complementary target oligonucleotides; the distance between CNT and QD highly depends on the length of the oligonucleotides, as observed in experiments; CNTs can quench the fluorescence signal of QDs; and the dynamic quenching and PL resonance energy transfer between CNTs and QDs should be responsible for the phenomena. When the CNT-QD method is used to detect the DNA or antigen molecules, the ratio of the CNT and QD probes is very important. According to our experience, 1:1 is suitable for almost all detected samples. When the sample concentration is lower than the concentration of the CNT and QD probes, part CNT probe and QD probe will be redundant because the distance between uncomplementary CNT probe and QD probe is far more than 10 nm. Therefore, the quenching degree of the QD probe caused by the CNT probe is much less, and the quenching degree can be detected as a control group. By measuring these gradually diluted samples with known concentration, the dose-effects standard curve can be set up before the samples with unknown concentration are detected. Therefore, the redundant CNT probes do not affect the final result of the detected samples.

Regarding the specificity and efficiency of the CNT-QD method, as is known, oligonucleotide hybridization has been broadly used for genetic diagnosis, chip detection, and so on. Its specificity and hybridization efficiency have been confirmed. Therefore, in this work, we did not focus on investigating the specificity and efficiency of the CNT-QD method. Our further work will evaluate its specificity and dynamic efficiency based on one-, two-, and three-base-pair mismatch probes and various temperature conditions as well as large quantities of background genomic and oligonucleotide existence as nonselective matrix effects.

Regarding the stability of the CNT and QD probes, asODN modified CNTs can enhance markedly the water solubility and dispersability of CNTs as reported (Zheng et al., 2003). We have also observed that the CNT probe is very stable at room temperature in PBS buffer for several months. The asODN-modified CdTe QDs are also water-soluble and very stable. Their PL intensities do not change at room temperature and in a dark environment for almost 2 years, and are almost not affected by different pH values, as reported (Pan et al.,

2008). Conversely, the PL intensity of unmodified QDs can be affected seriously by different pH values.

7. Conclusions and future prospects

In this section, we firstly designed a novel facile strategy to assemble CNTs and QDs in common aqueous solution based on a simple electrostatic interaction between amine-terminated CNTs and carboxyl-capped CdSe QDs. Individual QD was separately coated on the CNT surface to form CNT-QD nanocomplexes; as a result, PL of QDs can be quenched by CNT. Increasing of the CNT concentration led to the decrease of the PL intensity of QDs. The Stern-Volmer equation and doublelogarithmic equation were successfully used to calculate the quenching constant (K_{SV} and K_b) of CNT/QD systems, indicating that the interparticle space is the main parameter that determines the PL quenching constant, which can be explained by dynamic quenching and energy-transfer quenching mechanisms. Furthermore, quenching constants (K_{SV} and K_b) show little changes by varying pH values from 4.0 to 10.4, indicating a high quenching stability in different pH environments. Our results demonstrated that the dependent emissive properties of QDs coupled with CNTs opens a straightforward methodology for investigating the interaction between fluorescent molecules and other nanomaterials and further application in optical chemical sensors.

Based on the above novel facile strategy to assemble CNTs and QDs, we developed a novel and efficient DNA/protein detection method for biomolecules (such as oligonucleotide and antigen), that is based on DNA hybridization and antibody-antigen immunoreaction by using asODN-labeled CNTs and QDs as the molecular probes. The CNTs and QDs probes functionalized with alkyloligonucleotide can be assembled into a nanohybrid structure upon the addition of a target oligonucleotide. This strategy based on oligonucleotide hybridization assembly can be used to prepare multicomponent assembly materials comprising differently shaped oligonucleotide-functionalized nanomaterials. We have also developed a promising nanoscale CNTs probe and QDs probe for the direct, rapid, inexpensive, and sensitive detection and quantification of DNA/protein. Our probe combines the DNA hybridization and antigen-antibody interaction and is versatile and capable of simultaneous processing of multiple samples. The established method has great potential in applications such as ultrasensitive pathogen DNA or antigen or antibody detection, molecular imaging, and photoelectrical biosensors.

Based on the effects of MWNTs on the PL properties of CdSe QDs showed that CNTs could suppress the PL of QDs through both dynamic and energy transfer quenching mechanisms, a novel ultrasensitive DNA or antigen detection strategy by the CNT-QD assembly was designed for the direct, rapid, inexpensive, and sensitive detection and quantification of DNA/protein. Due to the DNA hybridization and antigen-antibody interaction and is versatile, simultaneous processing of multiple samples and higher assay throughput can be achieved. Nanotechnology provides a great opportunity to analytical chemists to develop better sensing strategies, but also relies on modern analytical techniques to pave its way to practical applications.

To sum up, nanomaterials are opening new horizons in the development of biosensor devices for simultaneous detection and measurement of specific multi-DNAs and antigens. Those biosensor devices could be useful for diagnosing and monitoring infectious diseases, monitoring the pharmokinetics of drugs, detecting cancer and disease biomarkers, analyzing breath, urine and blood for drugs of abuse, detecting biological and chemical

warfare agents, and monitoring pathogens in food, among other conceivable applications. The unique and attractive properties of nanomaterials can markedly improve the sensitivity, selectivity, specificity and rapidity of biomolecules detection, offer the promising capability of detecting or manipulating atoms and molecules, and have great potential in the development of the miniaturizability or portability analytical system.

8. Acknowledgements

9. References

Abu-Salah, K.M., Alrokyan, S.A., Khan, M.N., Ansari, A.A., 2010. Nanomaterials as analytical tools for genosensors. Sensors 10, 963-993.

Alivisatos, A.P., 1996. Semiconductor clusters, nanocrystals, and quantum dots. Science 271, 933.

Alivisatos, P., 2003. The use of nanocrystals in biological detection. Nature Biotechnology 22, 47-52.

Ao, L., Gao, F., Pan, B., He, R., Cui, D., 2006. Fluoroimmunoassay for antigen based on fluorescence quenching signal of gold nanoparticles. Analytical chemistry 78, 1104-1106.

Asefa, T., Duncan, C.T., Sharma, K.K., 2009. Recent advances in nanostructured chemosensors and biosensors. Analyst 134, 1980-1990.

Cataldo, F., 2008. Medicinal chemistry and pharmacological potential of fullerenes and carbon nanotubes. Springer Verlag.

Chan, W.C.W., Maxwell, D.J., Gao, X., Bailey, R.E., Han, M., Nie, S., 2002. Luminescent quantum dots for multiplexed biological detection and imaging. Current Opinion in Biotechnology 13, 40-46.

Chan, W.C.W., Nie, S., 1998. Quantum dot bioconjugates for ultrasensitive nonisotopic detection. Science 281, 2016.

Chen, R.J., Bangsaruntip, S., Drouvalakis, K.A., Wong Shi Kam, N., Shim, M., Li, Y., Kim, W., Utz, P.J., Dai, H., 2003. Noncovalent functionalization of carbon nanotubes for highly specific electronic biosensors. Proceedings of the National Academy of Sciences of the United States of America 100, 4984.

Cheung, C.L., Wong, S.S., Joselevich, E., Woolley, A.T., Lieber, C., 1998. Covalently functionalized nanotubes as nanometer-sized probes in chemistry and biology. Nature 394, 52-55.

Clapp, A.R., Medintz, I.L., Mauro, J.M., Fisher, B.R., Bawendi, M.G., Mattoussi, H., 2004. Fluorescence resonance energy transfer between quantum dot donors and dye-labeled protein acceptors. Journal of the American Chemical Society 126, 301-310.

Cooper, M.A., 2002. Optical biosensors in drug discovery. Nature Reviews Drug Discovery 1, 515-528.

Cui, D., 2007. Advances and prospects on biomolecules functionalized carbon nanotubes. Journal of Nanoscience and Nanotechnology, 7 4, 1298-1314.

Cui, D., Han, Y., Li, Z., Song, H., Wang, K., He, R., Liu, B., Liu, H., Bao, C., Huang, P., 2009. Fluorescent magnetic nanoprobes for in vivo targeted imaging and hyperthermia therapy of prostate cancer. Nano Biomed Eng 1, 61-74.

Cui, D., Jin, G., Gao, T., Sun, T., Tian, F., Estrada, G.G., Gao, H., Sarai, A., 2004a. Characterization of BRCAA1 and its novel antigen epitope identification. Cancer Epidemiology Biomarkers & Prevention 13, 1136.

Cui, D., Pan, B., Zhang, H., Gao, F., Wu, R., Wang, J., He, R., Asahi, T., 2008. Self-assembly of quantum dots and carbon nanotubes for ultrasensitive DNA and antigen detection. Analytical chemistry 80, 7996-8001.

Cui, D., Tian, F., Kong, Y., Titushikin, I., Gao, H., 2004b. Effects of single-walled carbon nanotubes on the polymerase chain reaction. Nanotechnology 15, 154.

Cui, D., Zhang, H., Sheng, J., Wang, Z., Toru, A., He, R., Gao, F., Cho, H.S.C.S., Huth, C., Hu, H., 2010. Effects of CdSe/ZnS Quantum Dots covered Multi-walled Carbon Nanotubes on Murine Embryonic Stem Cells. Nano Biomed Eng 2, 246-256.

Dai, H., 2002. Carbon nanotubes: synthesis, integration, and properties. Accounts of chemical research 35, 1035-1044.

Drbohlavova, J., Adam, V., Kizek, R., Hubalek, J., 2009. Quantum dots¡ᵃcharacterization, preparation and usage in biological systems. International Journal of Molecular Sciences 10, 656.

Edgar, R., McKinstry, M., Hwang, J., Oppenheim, A.B., Fekete, R.A., Giulian, G., Merril, C., Nagashima, K., Adhya, S., 2006. High-sensitivity bacterial detection using biotin-tagged phage and quantum-dot nanocomplexes. Proceedings of the National Academy of Sciences of the United States of America 103, 4841.

Elghanian, R., Storhoff, J.J., Mucic, R.C., Letsinger, R.L., Mirkin, C.A., 1997. Selective colorimetric detection of polynucleotides based on the distance-dependent optical properties of gold nanoparticles. Science 277, 1078.

Fan, L.J., Jones Jr, W.E., 2006. Studies of Photoinduced Electron Transfer and Energy Migration in a Conjugated Polymer System for Fluorescence Turn-On¡± Chemosensor Applications. The Journal of Physical Chemistry B 110, 7777-7782.

Gao, X., Yang, L., Petros, J.A., Marshall, F.F., Simons, J.W., Nie, S., 2005. In vivo molecular and cellular imaging with quantum dots. Current Opinion in Biotechnology 16, 63-72.

Genin, E., Carion, O., Mahler, B., Dubertret, B., Arhel, N., Charneau, P., Doris, E., Mioskowski, C., 2008. CrAsH- Quantum Dot Nanohybrids for Smart Targeting of Proteins. Journal of the American Chemical Society 130, 8596-8597.

Grzelczak, M., Correa-Duarte, M.A., Salgueirino-Maceira, V., Giersig, M., Diaz, R., Liz-Marzan, L.M., 2006. Photoluminescence Quenching Control in Quantum Dot-Carbon Nanotube Composite Colloids Using a Silica-Shell Spacer. Advanced Materials 18, 415-420.

Guldi, D.M., Rahman, G.M.A., Sgobba, V., Kotov, N.A., Bonifazi, D., Prato, M., 2006. CNT-CdTe versatile donor-acceptor nanohybrids. Journal of the American Chemical Society 128, 2315-2323.

Guldi, D.M., Zilbermann, I., Anderson, G., Kotov, N.A., Tagmatarchis, N., Prato, M., 2005. Nanosized inorganic/organic composites for solar energy conversion. Journal of Materials Chemistry 15, 114-118.

Guo, Y., Shi, D., Cho, H., Dong, Z., Kulkarni, A., Pauletti, G.M., Wang, W., Lian, J., Liu, W., Ren, L., 2008. In vivo Imaging and Drug Storage by Quantum©\Dot©\Conjugated Carbon Nanotubes. Advanced Functional Materials 18, 2489-2497.

Han, M., Gao, X., Su, J.Z., Nie, S., 2001. Quantum-dot-tagged microbeads for multiplexed optical coding of biomolecules. Nature Biotechnology 19, 631-635.

Hatchett, D.W., Josowicz, M., 2008. Composites of intrinsically conducting polymers as sensing nanomaterials. Chemical reviews 108, 746-769.

Hu, L., Zhao, Y.L., Ryu, K., Zhou, C., Stoddart, J.F., Gruner, G., 2008. Light-Induced Charge Transfer in Pyrene/CdSe-SWNT Hybrids. Advanced Materials 20, 939-946.

Huang, P., Wang, K., Pandoli, O., Zhang, X., Gao, F., Shao, J., You, X., He, R., Song, H., Cui, D., 2010. Fluoroimmunoassay for antigen based on fluorescence quenching between quantum dots and gold nanoparticles (Proceedings Paper).

Hwang, S.H., Moorefield, C.N., Wang, P., Jeong, K.U., Cheng, S.Z.D., Kotta, K.K., Newkome, G.R., 2006. Dendron-tethered and templated CdS quantum dots on single-walled carbon nanotubes. Journal of the American Chemical Society 128, 7505-7509.

Iijima, S., 1991. Helical microtubules of graphitic carbon. Nature 354, 56-58.

Jianrong, C., Yuqing, M., Nongyue, H., Xiaohua, W., Sijiao, L., 2004. Nanotechnology and biosensors. Biotechnology advances 22, 505-518.

Kamat, P.V., 2007. Meeting the clean energy demand: Nanostructure architectures for solar energy conversion. The Journal of Physical Chemistry C 111, 2834-2860.

Katz, E., Willner, I., 2004. Biomolecule-Functionalized Carbon Nanotubes: Applications in Nanobioelectronics. ChemPhysChem 5, 1084-1104.

Krishna, M.V.R., Friesner, R., 1991. Quantum confinement effects in semiconductor clusters. The Journal of Chemical Physics 95, 8309.

Kuhn, H., 1994. Reflections on biosystems motivating supramolecular engineering. Biosensors and Bioelectronics 9, 707-717.

Kumar, C.S.S.R., 2007. Nanomaterials for biosensors. Vch Verlagsgesellschaft Mbh.

Li, Q., Sun, B., Kinloch, I.A., Zhi, D., Sirringhaus, H., Windle, A.H., 2006a. Enhanced self-assembly of pyridine-capped CdSe nanocrystals on individual single-walled carbon nanotubes. Chemistry of materials 18, 164-168.

Li, W., Gao, C., Qian, H., Ren, J., Yan, D., 2006b. Multiamino-functionalized carbon nanotubes and their applications in loading quantum dots and magnetic nanoparticles. J. Mater. Chem. 16, 1852-1859.

Li, Z., Huang, P., He, R., Lin, J., Yang, S., Zhang, X., Ren, Q., Cui, D., 2010a. Aptamer-conjugated dendrimer-modified quantum dots for cancer cell targeting and imaging. Materials Letters 64, 375-378.

Li, Z., Huang, P., Lin, J., He, R., Liu, B., Zhang, X., Yang, S., Xi, P., Ren, Q., 2010b. Arginine-Glycine-Aspartic Acid-Conjugated Dendrimer-Modified Quantum Dots for Targeting and Imaging Melanoma. Journal of Nanoscience and Nanotechnology 10, 4859-4867.

Lin, Y., Taylor, S., Li, H., Fernando, K.A.S., Qu, L., Wang, W., Gu, L., Zhou, B., Sun, Y.P., 2004. Advances toward bioapplications of carbon nanotubes. J. Mater. Chem. 14, 527-541.

Liu, C., 2009. Research and development of nanopharmaceuticals in China. Nano Biomedicine and Engineering 1, 1-12.

Liu, Z., Tabakman, S., Welsher, K., Dai, H., 2009. Carbon nanotubes in biology and medicine: in vitro and in vivo detection, imaging and drug delivery. Nano research 2, 85-120.

Maurel, V., Laferri¨re, M., Billone, P., Godin, R., Scaiano, J., 2006. Free radical sensor based on CdSe quantum dots with added 4-amino-2, 2, 6, 6-tetramethylpiperidine oxide functionality. The Journal of Physical Chemistry B 110, 16353-16358.

Medintz, I.L., Clapp, A.R., Mattoussi, H., Goldman, E.R., Fisher, B., Mauro, J.M., 2003. Self-assembled nanoscale biosensors based on quantum dot FRET donors. Nature materials 2, 630-638.

Medintz, I.L., Uyeda, H.T., Goldman, E.R., Mattoussi, H., 2005. Quantum dot bioconjugates for imaging, labelling and sensing. Nature materials 4, 435-446.

Nam, J.M., Park, S.J., Mirkin, C.A., 2002. Bio-barcodes based on oligonucleotide-modified nanoparticles. Journal of the American Chemical Society 124, 3820-3821.

Nam, J.M., Thaxton, C.S., Mirkin, C.A., 2003. Nanoparticle-based bio-bar codes for the ultrasensitive detection of proteins. Science 301, 1884.

Niemeyer, C.M., 2001. Nanoparticles, proteins, and nucleic acids: biotechnology meets materials science. Angew. Chem. Int. Ed 40, 4128-4158.

Nirmal, M., Brus, L., 1999. Luminescence photophysics in semiconductor nanocrystals. Accounts of chemical research 32, 407-414.

Oh, E., Hong, M.Y., Lee, D., Nam, S.H., Yoon, H.C., Kim, H.S., 2005. Inhibition assay of biomolecules based on fluorescence resonance energy transfer (FRET) between quantum dots and gold nanoparticles. Journal of the American Chemical Society 127, 3270-3271.

Ornberg, R.L., Harper, T.F., Liu, H., 2005. Western blot analysis with quantum dot fluorescence technology: a sensitive and quantitative method for multiplexed proteomics. Nature Methods 2, 79-81.

Pan, B., Ao, L., Gao, F., Tian, H., He, R., Cui, D., 2005. End-to-end self-assembly and colorimetric characterization of gold nanorods and nanospheres via oligonucleotide hybridization. Nanotechnology 16, 1776.

Pan, B., Cui, D., Gao, F., He, R., 2006a. Growth of multi-amine terminated poly (amidoamine) dendrimers on the surface of carbon nanotubes. Nanotechnology 17, 2483.

Pan, B., Cui, D., He, R., Gao, F., Zhang, Y., 2006b. Covalent attachment of quantum dot on carbon nanotubes. Chemical physics letters 417, 419-424.

Pan, B., Cui, D., Ozkan, C.S., Ozkan, M., Xu, P., Huang, T., Liu, F., Chen, H., Li, Q., He, R., 2008. Effects of carbon nanotubes on photoluminescence properties of quantum dots. The Journal of Physical Chemistry C 112, 939-944.

Pan, B., Cui, D., Xu, P., Ozkan, C., Feng, G., Ozkan, M., Huang, T., Chu, B., Li, Q., He, R., 2009. Synthesis and characterization of polyamidoamine dendrimer-coated multi-walled carbon nanotubes and their application in gene delivery systems. Nanotechnology 20, 125101.

Pan, B., Gao, F., He, R., Cui, D., Zhang, Y., 2006c. Study on interaction between poly (amidoamine) dendrimer and CdSe nanocrystal in chloroform. Journal of colloid and interface science 297, 151-156.

Pandey, P., Datta, M., Malhotra, B., 2008. Prospects of nanomaterials in biosensors. Analytical Letters 41, 159-209.

Patolsky, F., Gill, R., Weizmann, Y., Mokari, T., Banin, U., Willner, I., 2003. Lighting-up the dynamics of telomerization and DNA replication by CdSe-ZnS quantum dots. Journal of the American Chemical Society 125, 13918-13919.

Peng, X., Manna, L., Yang, W., Wickham, J., Scher, E., Kadavanich, A., Alivisatos, A., 2000. Shape control of CdSe nanocrystals. Nature 404, 59-61.

Pradhan, N., Goorskey, D., Thessing, J., Peng, X., 2005. An alternative of CdSe nanocrystal emitters: pure and tunable impurity emissions in ZnSe nanocrystals. Journal of the American Chemical Society 127, 17586-17587.

Robel, I., Bunker, B.A., Kamat, P.V., 2005. Single-Walled Carbon Nanotube-CdS Nanocomposites as Light-Harvesting Assemblies: Photoinduced Charge-Transfer Interactions. Advanced Materials 17, 2458-2463.

Sheehan, P.E., Whitman, L.J., 2005. Detection limits for nanoscale biosensors. Nano letters 5, 803-807.

Sheeney-Haj-Ichia, L., Basnar, B., Willner, I., 2005. Efficient generation of photocurrents by using CdS/carbon nanotube assemblies on electrodes. Angewandte Chemie International Edition 44, 78-83.

Shi, D., Lian, J., Wang, W., Liu, G., He, P., Dong, Z., Wang, L.M., Ewing, R.C., 2006. Luminescent carbon nanotubes by surface functionalization. Advanced Materials 18, 189-193.

Si, H.Y., Liu, C.H., Xu, H., Wang, T.M., Zhang, H.L., 2009. Shell-Controlled Photoluminescence in CdSe/CNT Nanohybrids. Nanoscale research letters 4, 1146-1152.

Sittampalam, G.S., Kahl, S.D., Janzen, W.P., 1997. High-throughput screening: advances in assay technologies. Current Opinion in Chemical Biology 1, 384-391.

Slowing, I.I., Trewyn, B.G., Giri, S., Lin, V.S.Y., 2007. Mesoporous silica nanoparticles for drug delivery and biosensing applications. Advanced Functional Materials 17, 1225-1236.

So, H.M., Won, K., Kim, Y.H., Kim, B.K., Ryu, B.H., Na, P.S., Kim, H., Lee, J.O., 2005. Single-walled carbon nanotube biosensors using aptamers as molecular recognition elements. Journal of the American Chemical Society 127, 11906-11907.

Spichiger-Keller, U.E., 1998. Chemical Sensors and Biosensors for Medical and BiologicalApplications. Data Processing 1, 1.

Strehlitz, B., Nikolaus, N., Stoltenburg, R., 2008. Protein detection with aptamer biosensors. Sensors 8, 4296-4307.

Turner, A.P.F., 2000. Biosensors--sense and sensitivity. Science 290, 1315.

Turner, A.P.F., Karube, I., Wilson, G.S., 1987. Biosensors: fundamentals and applications. Oxford University Press, USA.

Valcarcel, M., Cardenas, S., Simonet, B., 2007. Role of carbon nanotubes in analytical science. Analytical chemistry 79, 4788-4797.

Valcarcel, M., Simonet, B., Cardenas, S., 2008. Analytical nanoscience and nanotechnology today and tomorrow. Analytical and Bioanalytical Chemistry 391, 1881-1887.

Valcarcel, M., Simonet, B.M., Cardenas, S., Suarez, B., 2005. Present and future applications of carbon nanotubes to analytical science. Analytical and Bioanalytical Chemistry 382, 1783-1790.

Vamvakaki, V., Chaniotakis, N.A., 2007. Carbon nanostructures as transducers in biosensors. Sensors and Actuators B: Chemical 126, 193-197.

Wang, X., Guo, X., 2009. Ultrasensitive Pb2+ detection based on fluorescence resonance energy transfer (FRET) between quantum dots and gold nanoparticles. Analyst 134, 1348-1354.

Xing, Y., Chaudry, Q., Shen, C., Kong, K.Y., Zhau, H.E., Chung, L.W., Petros, J.A., O'Regan, R.M., Yezhelyev, M.V., Simons, J.W., 2007. Bioconjugated quantum dots for multiplexed and quantitative immunohistochemistry. Nature Protocols 2, 1152-1165.

Yamada, N., Ozawa, S., Kageyama, N., Miyano, H., 2004. Detection and quantification of protein residues in food grade amino acids and nucleic acids using a Dot-Blot fluorescent staining method. Journal of agricultural and food chemistry 52, 5329-5333.

Yang, H., Guo, Q., He, R., Li, D., Zhang, X., Bao, C., Hu, H., Cui, D., 2009. A quick and parallel analytical method based on quantum dots labeling for ToRCH-related antibodies. Nanoscale research letters 4, 1469-1474.

Yang, H., Li, D., He, R., Guo, Q., Wang, K., Zhang, X., Huang, P., Cui, D., 2010a. A Novel Quantum Dots-Based Point of Care Test for Syphilis. Nanoscale research letters 5, 875-881.

Yang, R., Tang, Z., Yan, J., Kang, H., Kim, Y., Zhu, Z., Tan, W., 2008. Noncovalent assembly of carbon nanotubes and single-stranded DNA: an effective sensing platform for probing biomolecular interactions. Analytical chemistry 80, 7408-7413.

Yang, W., Ratinac, K.R., Ringer, S.P., Thordarson, P., Gooding, J.J., Braet, F., 2010b. Carbon Nanomaterials in Biosensors: Should You Use Nanotubes or Graphene? Angewandte Chemie International Edition 49, 2114-2138.

Zhang, F., Ali, Z., Amin, F., Riedinger, A., Parak, W.J., 2010. In vitro and intracellular sensing by using the photoluminescence of quantum dots. Analytical and Bioanalytical Chemistry 397, 935-942.

Zhang, X., Guo, Q., Cui, D., 2009. Recent advances in nanotechnology applied to biosensors. Sensors 9, 1033-1053.

Zheng, M., Jagota, A., Semke, E.D., Diner, B.A., McLean, R.S., Lustig, S.R., Richardson, R.E., Tassi, N.G., 2003. DNA-assisted dispersion and separation of carbon nanotubes. Nature materials 2, 338-342.

Zhong, W., 2009. Nanomaterials in fluorescence-based biosensing. Analytical and Bioanalytical Chemistry 394, 47-59.
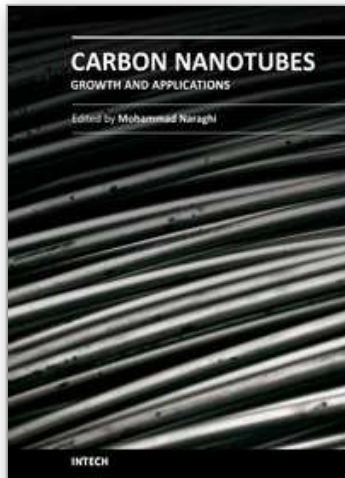
Carbon Nanotubes - Growth and Applications

Edited by Dr. Mohammad Naraghi

Carbon Nanotubes are among the strongest, toughest, and most stiff materials found on earth. Moreover, they have remarkable electrical and thermal properties, which make them suitable for many applications including nanocomposites, electronics, and chemical detection devices. This book is the effort of many scientists and researchers all over the world to bring an anthology of recent developments in the field of nanotechnology and more specifically CNTs. In this book you will find:
- Recent developments in the growth of CNTs
- Methods to modify the surfaces of CNTs and decorate their surfaces for specific applications
- Applications of CNTs in biocomposites such as in orthopedic bone cement
- Application of CNTs as chemical sensors
- CNTs for fuelcells
- Health related issues when using CNTs

How to reference

In order to correctly reference this scholarly work, feel free to copy and paste the following:

Peng Huang and Daxiang Cui (2011). Simultaneous Detection of Multi-DNAs and Antigens Based on Self-Assembly of Quantum Dots and Carbon Nanotubes, Carbon Nanotubes - Growth and Applications, Dr. Mohammad Naraghi (Ed.), ISBN: 978-953-307-566-2, InTech, Available from:
http://www.intechopen.com/books/carbon-nanotubes-growth-and-applications/simultaneous-detection-of-multi-dnas-and-antigens-based-on-self-assembly-of-quantum-dots-and-carbon-

INTECH
open science | open minds